HHS Public Access

Author manuscript

Biomaterials. Author manuscript; available in PMC 2019 October 01.

Published in final edited form as:

Biomaterials. 2018 October ; 180: 225–239. doi:10.1016/j.biomaterials.2018.07.026.

Melatonin Improves Quality and Longevity of Chronic Neural Recording

Asiyeh Golabchi[1,2], **Bingchen Wu**[1,2], **Xia Li**[1], **Diane L. Carlisle**[4], **Takashi D. Y. Kozai**[1,2,3,5], **Robert M. Friedlander**[4], and **Xinyan Tracy Cui**[1,2,3,*]

[1]Department of Bioengineering, University of Pittsburgh.

[2]Center for Neural Basis of Cognition.

[3]McGowan Institute for Regenerative Medicine, University of Pittsburgh.

[4]Neuroapoptosis Laboratory, Department of Neurological Surgery, University of Pittsburgh School of Medicine.

[5]Neurotechnology Division of the University of Pittsburgh Brain Institute.

Abstract

The chronic performance of implantable neural electrodes is hindered by inflammatory brain tissue responses, including microglia activation, glial scarring, and neuronal loss. Melatonin (MT) has shown remarkable neuroprotective and neurorestorative effects in treating central nervous system (CNS) injuries and degeneration by inhibiting caspase−1, −3 and −9 activation and mitochondrial cytochrome c release, as well as reducing oxidative stress and neuroinflammation. This study examined the effect of MT administration on the quality and longevity of neural recording from implanted microelectrode in the visual cortex of mice for 16 weeks. MT (30 mg/kg) was administered via daily intraperitoneal injection for acute (3 days before and 14 days post implantation) and chronic (3 days before and 16 weeks post implantation) exposures. During the first 4 weeks, both MT groups showed significantly higher single-unit (SU) yield, signal-to-noise ratio (SNR), and amplitude compared to the vehicle control group. However, after 4 weeks of implantation, the SU yield of the acute treatment group dropped to the same level as control group, while the chronic treatment group maintained significantly higher SU yield compared to both acute (week 5–16) and control (week 0–16) mice. Histological studies revealed a significant increase in neuronal viability and decrease in neuronal apoptosis around implanted electrode at

*Corresponding author: X. Tracy Cui, Ph.D., Department of Bioengineering, University of Pittsburgh, 5057 Biomedical Science Tower 3, 3501 Fifth Avenue, Pittsburgh, PA 15260, Ph: 412-383-6672, Fx: 412-648-9076, xic11@pitt.edu.

Author contributions: A.G. carried out the experiments and analyzed the data. B.W. helped with daily MT injection. X.L. worked on histological tissue preparation. A.G. wrote the manuscript with input from all authors. T.K. and X.T.C. supervised data collection and analysis. D.C. and R.F. provided expertise on MT's biological mechanisms. X.T.C. and R.F. conceived the original idea. X.T.C. supervised the project.

Competing interests: The authors have no conflict of interest related to this research to disclose.

Data and materials availability: The datasets generated during and/or analyzed during the current study are available from the corresponding author on reasonable request.

week 16 in the chronic group in comparison to control and acute subjects, which is correlated with reduced oxidative stress and increased number of pro-regeneration arginase-1 positive microglia cells. These results demonstrate the potent effect of MT treatment in maintaining a high quality electrode-tissue interface and suggest that MT promotes neuroprotection possibly through its anti-apoptotic, anti-inflammatory and anti-oxidative properties.

One Sentence Summary:

This study demonstrated the potent effect of melatonin treatment in inhibiting persistent inflammation and neuronal loss, as well as maintaining high quality neural recording in chronic microelectrode brain implantation.

Keywords

Melatonin; antioxidant; single-unit recording; microelectrode arrays; oxidative stress; inflammatory gliosis

1. Introduction

Neural interface technologies utilize neural recording and/or stimulation to monitor or restore sensory or motor function [1–3]. Penetrating microelectrode arrays enable recording of SU spike activity and multi-unit (MU) activity from populations of neurons to investigate neuronal network dynamics [4, 5]. Furthermore, engaging an implantable neural interface to translate the recorded motor commands of paralyzed patients into controlling external devices or providing sensory feedbacks via stimulation demonstrates the tremendous potential of brain-computer interfaces for several clinical applications [6–8].

Achieving a high quality long-term performance from such implanted electrodes is one of the most challenging problems in the field. Many studies have reported significant SU amplitude decrease over time [9–11], and the degradation in signal quality leads to the drop in single-unit yield over time [9, 12]. The chronic failure has been contributed to both material degradation and biological host tissue responses [13–17]. The penetrating injury damages neurons in the implant path and decrease the neural density around the implantation site. Reduced neuronal density near the electrodes will consequently lead to reduced recording performance [15]. The implantation also inevitably damages the vasculature and blood brain barrier (BBB) and activates microglia/macrophages and subsequently astrocytes, which orchestrate the inflammatory response. Over time, microglia, astrocytes, and NG2 glia ensheath the implant, and the electrode from surrounding brain tissue and release high levels of pro-inflammatory cytokines such as interleukin-1β (IL-1β), tumor necrosis factor (TNF-α) and monocyte chemoattractant protein-1 (MCP-1), as well as reactive oxygen and nitrogen species (RONS) [14, 18–21]. Persistent release of these factors cause chronic inflammation which results in a glial encapsulation layer ranges that from 50 to 400 μm in diameter [22]. Chronic inflammation could also compromise neuronal function by neuronal degeneration and demyelination [7, 17, 19, 23–26]. Indeed degenerating neural processes near the kill zone are observed over long implantation periods similar to what has been observed in neurodegenerative disorders [27], which may lead to signal degradation

over time. Recently, studies focused on understanding the cellular pathways leading to implant-induced tissue responses have emerged using transgenic knockout and molecular analyses [26, 28]. By knocking out caspase-1, a mediator of both apoptosis and inflammation, neural recording performance was significantly improved [26]. These studies provided useful information for targeted therapies.

Among the multiple therapeutics targeting inflammation and neuronal death, MT is an attractive candidate. A hormone known for its role in circadian rhythm in regulating sleep, MT also has remarkable neuroprotective and neurorestorative effects in treating CNS injuries and degeneration. MT easily diffuses through biological membranes and the BBB and has multiple beneficial properties such as anti-inflammation [29–31], anti-oxidant [32–34] and anti-apoptotic [35] effects. MT as a regulator of the inflammatory cell compartment exerts cyto-protective actions by regulating oxidative stress, and altering leukocytes proliferation, apoptosis and mitochondrial homeostasis [36, 37] and has shown therapeutic effects in CNS diseases such as Alzheimers Disease, Parkinson's Disease, multiple sclerosis, stroke, Huntington's disease, amyotrophic lateral sclerosis (ALS) and brain ischemia/reperfusion [38–41]. MT acts both receptor-dependently by interacting with plasma membrane (MT1/MT2), mitochondrial (MT1) and nuclear orphan (ROR/RZR) receptors, as well as receptor-independently based on its free radical scavenging property [38, 41]. We have recently demonstrated a mitocrine pathway where MT is synthetized in neuronal mitochondrial matrix, released and by binding to the MT1 receptor it inhibits cytochrome c release and activation of the caspase cell death pathways [41]. MT can enter mitochondria where it scavenges free radicals [42, 43] and prevents molecular damage resulting from toxic RONS [38]. Several studies have demonstrated the protective role of MT as an antioxidant in reducing apoptosis both *in vivo* and *in vitro* [44–48]. For example, MT protects neurons from excitotoxicity and apoptotic cell death by controlling free radical processes [44]. Regardless of the mechanism (receptor dependent or not), MT inhibits the production of inflammatory cytokines including TNF-α, IL-1β, or interleukin-6 (IL-6) via different pathways [49–52] by suppressing macrophage cyclooxygenase-2 and inducible nitric oxide synthase (iNOS) [53], as well as blocking the transcriptional factors that stimulate pro-inflammatory cytokine production [54]. Furthermore, MT inhibits the activation of NF-KB [55, 56] and the caspase-1/cytochrome *c*/caspase-3 cell death pathway during inflammation [29, 30, 40, 57, 58].

With these considerations in mind, we hypothesized that MT administration may improve neural recording quality and longevity for chronically implanted electrodes by inhibiting inflammatory responses and decreasing neuronal loss and degeneration. We investigated the effects of daily MT administration, which includes an acute administration (3 days prior to implant and continuing for 14 days after surgery) and chronic treatment (3 days prior to implant until the end time point of the study, 16 weeks), on neural recording performance and host tissue responses of implanted neural electrode arrays.

2. Materials and Methods

This study compares the neural recording characteristics of intracortical microelectrode arrays implanted in acute MT-treated (daily injection 3 days before and 2 weeks after

implantation, chronic MT (daily injection 3 days before and 16 weeks after implantation) and vehicle control in C57BJ/6 wild type (WT) mice. A visually evoked cortical recording model was used [59–61], and recording performance was evaluated through single-unit yield, single-unit signal to noise ratio, single-unit amplitude, noise floor and impedance using previously published methods [26, 62]. At the end time point (16W), postmortem immunohistochemistry was performed to examine the molecular, cellular, and vascular responses around the implantation site.

2.1. Animals and Surgical Implant Procedure

20 C57BL/6J male mice (age, 9 weeks; weight, 20 to 25 g; The Jackson Laboratory, Bar Harbor, ME) were kept in the temperature-controlled animal facility center (DLAR) in a ventilated rack at the University of Pittsburgh with a12:12-h light: dark cycle and with ad libitum access to food and water. All procedures were approved by the Institutional Animal Care and Use Committee of the University of Pittsburgh, in accordance with the guideline.

All animal surgeries were performed as previously described [26, 63]. 3 days before surgery, animals were allocated randomly into 3 groups; control (N=6, received saline by daily injection 3 days before and 16 weeks after implantation), acute MT (N=6, received MT by daily injection 3 days before and 2 weeks after implantation), chronic MT (N=8 (2 mice scarified at week 6 and 12 after surgery (failure of dental cement head-cap due to unstable interface between the skull and dental cement)), received MT by daily injection 3 days before and 16 weeks after implantation). Mice were anesthetized by using an Isoflurane Vaporizer (Patterson Veterinary Inc.; isoflurane inflow was 2% for induction phase and maintained at 1.5% during surgery) that provides a mixture of isoflurane and oxygen. A warm water pad (HTP 1500, Adroit Medical Systems, Loudon, TN) was set to 37 °C and placed underneath the anesthetized mouse to maintain body temperature. The mouse was mounted to the stereotaxic frame (Kopf Instruments, Tujunga, CA) and the skull was exposed. The hole was drilled in the skull with a surgical drill (0.007 drill bit, Fine Science Tools, Inc., Foster City, CA) over the 1 mm anterior to Lambda and 1.5 mm lateral to midline. Sterilized saline was applied continuously for cutting heat dissipation in high-speed drilling of the bone. Three sterilized bone screws (Stainless Steel; shaft diameter: 1.17 mm, length: 4.7 mm; Fine Science Tools, Inc., Foster City, CA) were screwed bilaterally over the primary motor cortex (as the grounding electrode) and over the contralateral visual cortex (as the reference electrode) for anchoring dental cement to bone. A functional 3 mm single-shank planar silicon probe with 15 μm thickness and 16-circularelectrode site with 30 μm diameter and 100 μm site-spacing (NeuroNexus, Ann Arbor, MI, A1×16-3MM-100-703-CM15) were implanted in the left visual cortex using a stereotaxic manipulator until the top edge of the last electrode site is below the brain surface. After filling the craniotomy with Kwik-Cast Sealant (World Precision Instruments, Sarasota, FL), the reference and grounding wires were connected to the bone screws and dental cement (Pentron Clinical, Orange CA) was cured with a dental curing light to make a head-cap. After surgery, animals received intraperitoneal (i.p.) injection of 5mg/kg ketofen (100mg/ml, Zoetis Inc, Kalamazoo, MI) and placed on an electric heating blanket under a warming light to wake up. Daily use of analgesic continued for three days after surgery.

2.2. Pharmacological Treatment

MT (MP Biomedicals, Inc., Fisher scientific) was administered i.p. at a dose of 30 mg/kg (100μl) to the MT treated group (Figure 1 A). It was prepared in 0.9% saline after being dispersed by dimethyl sulfoxide (DMSO) fresh daily. The daily injection was started 3 days before and continued for 2 weeks (acute MT) or 16 weeks (chronic MT) after implantation. This is an effective dose identified in the previous study for treating ALS disease [64]. Control groups received saline injection following the same schedule as the chronic MT group. For the control and the acute MT: $N = 6$ for 1–120 days. For the chronic MT group: $N = 8$ for 1–42 days, $N = 7$ for 43–84 days, and $N = 6$ for 84–120 days.

2.3. Neurophysiological Recording

Recording of spontaneous and visually evoked SU, MU and local field potential (LFP) responses was performed each week as extensively described [26, 62, 63] under 1% isoflurane anesthesia (Figure 1 B). Briefly, electrophysiological recording was conducted from the animal inside of a Faraday cage in a dark room. Visual stimuli were presented by using the MATLAB-based Psychophysics toolbox [59, 60, 65] through a 24” LCD (V243H, Acer. Xizhi, New Taipei City, Taiwan) located outside of cage and placed 20 cm from the eye contralateral to the implant. Solid black and white bar gratings were presented drifting in a perpendicular direction and synchronized with the recording system (RX7, Tucker-Davis Technologies, Alachua FL) at 24.414 Hz. The raw data stream was filtered to produce spike (0.3 to 5 kHz) data streams. Further, the spike data stream was pre-processed through previously published methods [66, 67] and individual units were identified by using a fixed negative threshold value of 3.5 SD [26, 66]. Offline spike sorting was performed through a custom MATLAB script modified from previously mentioned methods [62, 63, 68]. To quantify the single-unit quality, the average signal-to-noise amplitude ratio (averaging the amplitudes of single-units for each channel) and the average amplitude of noise (2 SD) were calculated. Only candidate units with detectable spikes (SNR >2) were analyzed. Channels with SNR between 2 and 3 were manually selected by examining the combination of waveform shape, auto-correlogram, peak threshold crossing offset, and peri-stimulus time histogram (PSTH) with 50 ms bins and candidate units with SNR greater than 3 were manually confirmed by examining the waveform shape [26]. Additionally, we quantified the MU Signal-to-Noise Firing Rate Ratio (SNFRR) as the average firing rate of the ‘ON’ state minus the average firing rate of the ‘OFF’ state to the visual trigger divided by the average standard deviation of the ‘ON’ and ‘OFF’ state both [63]. Furthermore, we quantified the spike firing rate of SU and MU activity in the resting state between different treatment conditions to evaluate the activity and excitability of the neurons.

2.4. Electrochemical Impedance Spectroscopy (EIS)

EIS was used to characterize the electrode properties and glial scar encapsulation. Data was collected before implantation and after every recording session under anesthesia (1.5% isoflurane) through connecting implanted electrode to an Autolab potentiostat using a 16 channel multiplexer. A voltage of 10 mV RMS sine wave from 10–32,000 Hz was applied to measure EIS, using individual electrode sites as the working electrodes and stainless steel screw (19010–00, Fine Science Tools, Inc., Foster City, CA) as the counter electrode.

2.5. Immunohistochemistry

According to University of Pittsburgh IACUC approved methods, mice were sacrificed at the end (16 weeks). Each animal was deeply anesthetized using 80–100 mg/kg ketamine, 5–10 mg/kg xylazine cocktail. Once mice were unresponsive to tail/toe pinches, animals were transcardially perfused using phosphate buffered saline (PBS) flush at <80 mmHg followed by 4% paraformaldehyde (PFA) at <80 mmHg. Mice were decapitated and the skulls were removed to post-fix the brain in a 4% PFA at 4 °C for 4–6 h. Then, brains were soaked in a 15% sucrose (Sigma-Aldrich Corp., St. Louis, Missouri) bath at 4 °C overnight followed by a 30% sucrose solution for 24 h. Brains were then carefully frozen in a 2:1 20% sucrose in PBS:optimal cutting temperature compound (Tissue—Plus O.C.T. Compound, Fisher HealthCare, Houston, TX) blocking media blend with dry ice. Frozen tissue was then horizontally sectioned into 25 μm thick sections normal to the tract of the probes using a cryostat (Leica CM1950, Buffalo Grove, IL).

Cortical sections of implanted and non-implanted hemisphere were mounted on the same slide for comparison and staining for each antibody combination was performed at the same time to minimize variability. Antibodies to visualize neurons (NeuN, 1:250, MAB377 Millipore), apoptotic cell death (cleaved caspase-3, 1:500, 9661S Cell Signaling), microglia (Iba-1, 1:500, NC9288364, Fisher), astrocytes (GFAP, 1:500, Z033401 Dako), blood vessels (tomato-plant lectin, 1:250, B1175 Vector Labs), M1 macrophage (iNOS, 1:250, 482728 Millipore), M2 macrophage (Arginas 1 (Arg1), 1:500, ABS535 Millipore), macrophage/microglia (ED-1, 1:100, ab31630 Abcam), lipid peroxidation (4-hydroxy-2-nonenal (4HNE), 1:200, 24325 Oxisresearch) and/or blood-brain barrier injury (immunoglobulin G (IgG), 1:16, Alexa Flour 647-conjugated AffiniPure Fab Fragment goat anti-mouse IgG 115-607-003 Jackson ImmunoResearch Laboratories, Inc.) (antibodies outlined in Table 1) were used. These antibodies were used to investigate the effect of MT injection in glial activation, probe encapsulation, number of viable neurons and amount of free radicals.

Tissue sections were rehydrated in 1 × PBS for 2×5 min. The tissues were then incubated in 0.01 M sodium citrate buffer for 30 min at 60 °C. Then, a peroxidase block (PBS with 10% v/v methanol and 3% v/v hydrogen peroxide) was performed for 20 min at room temperature (RT) on a table shaker. Next, tissue sections were incubated in carrier solution (1 × PBS, 5% normal goat serum, 0.1% Triton X-100) for 30 min at RT. Lastly, the tissue sections were blocked with Alexa Flour 647-conjugated AffiniPure Fab Fragment goat anti-mouse IgG (IgG, 1:16, 115-607-003 Jackson ImmunoResearch Laboratories, Inc.) or Fab fragment only (1:13, 115-007-003, JacksonImmunoResearch Laboratories, Inc.) for 2 hours then rinsed 6 times each 4 minutes. Following blocking, sections incubated in a primary antibody solution consisting of carrier solution and antibodies listed in Table 1 overnight (12–18 hours) at RT were then washed with 1 × PBS for 3 × 5 min and incubated in carrier solution and secondary antibodies (1:500, Alexa Flour 488 goat-anti mouse, Invitrogen, and 1:500 Alexa Flour 568 goat-anti rabbit, Invitrogen, 1:500, DyLight 649 Streptavidin, Vector Labs, 1:500 Alexa Flour 568 goat-anti mouse, Invitrogen, 1:500 Alexa Flour 488 goat-anti rabbit, Invitrogen, 1:500 Alexa Flour 633 goat-anti chicken, Invitrogen) for 2 hours at RT. Then sections were rinsed with PBS for 3 × 5 min and exposed to Hoechst (1:1000, 33342

Invitrogen) for 10 min and washed in PBS for 3 × 5 min before being coverslipped with Fluoromount-G (Southern Biotech, Associate Birmingham, AL).

2.6. Quantitative tissue analysis

Sections were imaged using confocal fluorescent microscopy to evaluate the cellular reactions associated with the implanted electrodes. Images were acquired using an Olympus Fluoview FV-1000 Confocal Microscope (Olympus America, Center Valley, PA) at the Center for Biologic Imaging at the University of Pittsburgh. For each antibody, images were taken using the same laser power, exposure time, and detector settings to decrease variability. Images were centered on the implant site and multi-channel images were acquired simultaneously. For Iba-1, GFAP, tomato lectin, IgG, and 4HNE, images were analyzed using a pixel-based radial image intensity analysis, as previously described [69]. Sections in the range of 500 μm to 1000 μm depth from the brain surface were compared with control (non-implanted) sections. For each image, the center of insertion site was chosen and by using the MATLAB script, masks of concentric rings every 20 μm for 240 μm were generated. Then, MATLAB scrip calculated and normalized the average gray scale intensity for all pixels above the threshold of the background noise intensity in each 20 μm bin. Finally, intensities were averaged for each group (control, acute MT, chronic MT), and then bar graphs for intensity-based radial analysis of fluorescent markers were plotted by mean ± standard error as a function of distance.

For NeuN, Caspase 3, iNOS, Arg1, and ED-1, cells were manually counted in each bin and the cell density (cell count per tissue area) was calculated. As previously described, data were averaged for each group, and the bar graphs for density-based radial analysis of cells (the mean and standard error) were plotted as a function of distance to the implantation site.

2.7. Statistics

General linear model repeated measure ANOVA and Tukey's post hoc tests were conducted in SPSS to compare the effect of time and type of treatment on recording or tissue characteristics among three groups at the same time points. $p<0.05$ was deemed statistically significant. $N = 6$ for the control and the acute MT. For the chronic MT group: $N = 8$ for 1–6 weeks, $N = 7$ for 7–12 weeks, and $N = 6$ for 13–16 weeks.

3. Results

3.1. Electrode Performance Analysis

3.1.1. Depth Independent Chronic Electrode Performance Analysis—Electrical recording performance was measured by averaging performance metrics of all 16 channels along the Michigan probe shank. Visually evoked single-unit yield (percentage of recording sites able to detect a single-unit) is presented in Figure 2 A, which for the control group started acutely at 57± 8% and declined gradually to 31 ± 5% on week 3. After that, single-unit yield showed trivial inclination up to week 6 and subsequently, it remained steady for the remainder of the 16 weeks recording duration. On the other hand, the acute and chronic MT groups began with a yield of 71 ± 5% (acute MT) and 70 ± 4% (chronic MT) and declined to 56 ± 7% (acute MT) and 63 ± 5% (chronic MT) on week four. After two weeks

the SU yield of the acute MT group was significantly greater than the control group ($p<0.05$), however, after week 4, the SU yield of the acute MT group dropped and showed no significant difference with the control group. The electrodes in the chronic MT group had significant higher SU yield 6 hours post implant through the end time point of the study compared to the control (week 0 through 16, $p<0.05$). The comparison between the acute and chronic schedule showed that the chronic MT group showed significantly higher SU yield than the acute MT from week 4 onward. From week 6 on, single-unit yield from the control and acute treated groups had decreased to an average of four and five sites per array, respectively, and remained steady for the remaining implantation period of 16 weeks. On the contrary, the chronic MT group maintained significantly higher SU yield compared to both the acute MT and control mice over 5–16 weeks of implantation (Figure 2 A).

In addition, average SNR (signal-to-noise ratio defined as single-unit amplitude/2× standard deviation) of SUs also showed significant difference between the chronic MT treated group and control animals from 6 hours to 16 weeks post-implantation ($p<0.05$) (Figure 2 B). Also, from week 4 onward, the chronic MT group presented higher SNR compared to the acute MT group ($p<0.05$). Mean single-unit SNR began at 2.36 ± 0.54 for the control, 4.34 ± 0.93 for the acute and 3.27 ± 0.66 for the chronic treated groups (channels with no detectable single-units were considered to have SNR = 0), then declined to 1.01 ± 0.38 (control), 1.83 ± 0.43 (acute MT) and 2.20 ± 0.50 (chronic MT) on week 4 where it stabilized. In general, when electrodes with no detectable SUs were excluded, the average SNR of the channels that were recording single-units was initially higher in MT groups compared to the control ($p<0.05$) but after that it remained almost the same for all groups ($p>0.05$) over 16 weeks of study (Figure 2 C). The average amplitude of the single-units started with amplitude of 35.22 ± 8.31 μV (control), 61.97 ± 13.67 μV (acute MT) and 42.39 ± 9.21 μV (chronic MT) on the implantation day and declined to 19.88 ± 7.66 μV (control) and 38.56 ± 9.35 μV (acute MT) on week four (Figure 2 D). Interestingly, the SU amplitude of the chronic treated group was almost the same six hours post-implantation but was significantly greater compared to the control group between week 1 and 16 ($p<0.05$). In addition, there were significant differences between the chronic MT and the acute MT groups at the majority of weeks tested during the 16 weeks of the study. Moreover, the acute MT group showed significantly higher signal amplitude compared to the control animals 6 hours post-implant and from week 2 to week 4 ($p<0.05$), while afterward it was almost the same as the control ($p>0.05$). The amplitude of noise floor was 13.78 ± 0.91 μV (control), 13.86 ± 0.54 μV (acute MT) and 12.75 ± 0.84 μV (chronic MT) on the surgery day, and increased to 16.06 ± 0.87 μV (control), 16.86 ± 0.65 μV (acute MT) and 16.85 ± 0.73 μV (chronic MT) on week one and remained stable (Figure 2 E). The impedance of implanted electrode sites at 1 kHz (the relevant frequency of neuronal action potential) is shown in Figure 2 F. The impedance at 1 kHz increased from 281.89 ± 16.93 kΩ (control), 199.49 ± 11.58 kΩ (acute MT), and 221.10 ± 16.32 kΩ (chronic MT) before implantation to 929.42 ± 72.42 kΩ (control), 395.41 ± 25.90 kΩ (acute MT), and 396.55 ± 26.26 kΩ (chronic MT) at the day of surgery and to 983.01 ± 95.60 kΩ (control), 938.49 ± 79.68 kΩ (acute MT), and 1020.91 ± 111.26 kΩ (chronic MT) by week 3 and then stabilized for all groups for the remaining implantation time. Significant differences were observed on the day of implantation between

the control and MT treated groups and on week 1 after implant between the chronic MT and control, while the noise amplitude was almost the same in all groups.

3.1.2. Depth Dependent Chronic Electrode Performance Analysis—The depths of implant were aligned across animals in each group at their average layer IV depth between week 2 and week 16 (Figure 3). Layer IV was recognized with current source density (CSD) following the visual stimulus. Acutely in control mice, electrodes at the depth of 300, 500, 600, and 1000 μm had high yield (above (80%), but in chronic time points, only electrodes at the depths of 500 μm (layer IV) and 900 μm (layer VI) had moderate recording yield (60%). In the acute MT group, the SU yield was initially high (above 80%) at the depth of 200 μm (layer II/III) and 500 μm (layer IV) through 800 μm (Layer VI), and 1100 μm. However, after four weeks, the yields drop significantly to about 50% at depth of 300 μm (layer II/III) and 700 μm (layer V), while even lower at other depth. In contrast, the chronic MT group showed maintained high SU yield across multiple depths throughout the 16 weeks.

3.2. Histology

3.2.1. Neuronal density and health around the implanted electrode—To investigate the neuronal density and health around the implanted area at week 16, NeuN staining was combined with cleaved caspase-3 staining and Hoechst to recognize neurons and cells undergoing neurodegeneration, in control (Figure 4 C), acute MT (Figure 4 F), and chronic MT (Figure 4 I), respectively [26]. In the control and acute MT groups, loss of neuronal density (Figure 4 A, D) and elevated caspase-3 activity (Figure 4 B, E) were detected around the implants consistent with lower electrophysiological activity. However, the chronic MT mice maintained good viable neural density around electrode, a healthy electrode interface, and strong electrophysiological recordings (Figure 4 G, H). Neuron density was quantified with an automated MATLAB script. The number of neurons around the implanted electrode in the control and acute MT group was almost the same ($p<0.05$). However, the chronic MT group showed almost 49% and 42% increase in the number of neurons per area at the distance of 0 μm-10 μm *($p=0.047$)* and 10 μm-30 μm *($p=0.008$)* compared to the control group (Figure 4 J). Also, the density of neuronal cell in the chronic MT group indicated a 43% increase compared to acute MT within 30 μm distance (*$p=0.008$*). Additionally, the number of caspase-3 positive neuronal cells around the chronic MT group was 70% lower than control in 10 μm away from electrode tissue interface, suggesting chronic MT treatment provide a healthy environment for neuronal survival in the chronic MT group compared to the control group (Figure 4 K; *$p=0.042$*). On the contrary, at 16 weeks, the number of caspase-3 positive neurons of the acute MT group is similar to the control ($p<0.05$).

3.2.2. Oxidative stress—To check the level of reactive oxygen species (ROS) around implanted area at week 16, we used 4HNE as a marker for lipid peroxidation, a product of ROS and Hoechst (Figure 5 D–F). As shown in Figure 5 A–C, the intensity of ROS is centered close to the implantation site. Notably, the intensity of 4HNE in the chronic MT group was 66% lower than control *($p=0.014$)* and 63% lower than the acute MT group *($p=0.009$)* within 10 μm of the implantation. (Figure 5 G). Moreover, the ROS level was

60% lower in the chronic MT group compared to the control group at 10 μm-30 μm distance (Figure 5 G; *p=0.043*). These results support the role of MT in decreasing the ROS level around implanted electrodes.

3.2.3. Chronic inflammatory tissue response—We comprehensively characterized the inflammatory cellular and vascular responses associated with the chronic implanted device at week 16. First, the distribution of IgG was investigated to monitor BBB permeability [70]. A lower amount of IgG leakage from vasculature was detected in both MT treated groups compared to the control group which corresponds with less microglia aggregation around the implantation site (Figure 6 A–C). The acute MT group yields 55% (0 μm-10 μm; *p=0.042*), and 56% (10 μm-30 μm; *p=0.022)* reduction in IgG leakage compared to the control (Figure 6 J). Meanwhile, the chronic MT group showed 54% (0 μm-10 μm; *p=0.038* lower intensity in BBB injury compared to the control group (Figure 6 J).

By co-labeling with tomato lectin, activated/reactive microglia in the damaged area of the brain can be recognized [71] along with blood vessels [72]. Although, the expression of tomato lectin around the implant revealed similar distribution of blood vessels at a short distance around the implants in all groups, increased intensity at the vicinity of the implants especially the control was observed (Figure 7 D–F). The lectin intensity in the acute MT yields 46% (0 μm-10 μm; *p<0.001*), 52% (10 μm-30 μm; *p=0.001*), 48% (30 μm-50 μm; *p=0.005*), and 23% (50 μm-70 μm; *p=0.008)* reduction compared to the control group (Figure 7 K). The expression of lectin around the implanted electrodes in the chronic MT group also appeared significantly lower than the control group within 70 μm of electrode-tissue interface (Figure 7 K). It yields 56% (0 μm-10 μm; *p<0.001*), 51% (10 μm-30 μm; *p=0.001*), 49% (30 μm-50 μm; *p=0.002*), and 25% (50 μm-70 μm; *p=0.004)* reduction of blood vessels and glial cell population in the chronic MT compared to the control group.

Moreover, the microglia response was further characterized in Figure 6 and Figure 8. Ionized calcium binding adaptor molecule (Iba-1) is a selective marker for both resting and activated microglia/macrophages [70]. Lower Iba-1 expression around both MT treated groups compared to control group was observed (Figure 6 E and F compared to Figure 6 D). This yields 34% (0 μm-10 μm; *p=0.004)* and 14% (10 μm-30 μm; *p=0.038)* reduction of Iba-1 intensity in the acute MT compared to control group (Figure 6 K). Also, the chronic MT presented 54% (0 μm-10 μm; *p=0.004)* and 36% (10 μm-30 μm; *p=0.024)* reduction in Iba-1 expression than the control (Figure 6 K). Figure 6 (G–I) shows co-localization of IgG, Iba-1, and Hoechst staining in the control, acute MT and chronic MT, respectively.

In response to injury, microglia/macrophages get activated to the different phenotypes (e.g. M1 or M2) with patholological and reparative potential to the injury [73, 74]. Next, to discriminate the MT effect on modulation of microglia/macrophage phenotypes, samples were stained with ED-1, a cytoplasmic antigen found only in activated monocytes and macrophages [75], iNOS (pro-inflammatory M1 marker), and Arg 1 (neuroprotective M2 marker) (Figure 8). ED-1 expression was only found to be localized to the insertion site (Figure 8 A–C). iNOS (Figure 8 D–F), Arg1 (Figure 8 G–I) and co-localization of ED-1, iNOS, Arg1, and Hoechst staining (Figure 8 J–L) for the control, acute MT, and chronic MT is shown in Figure 8. The density of activated macrophages around the implanted electrode

in the chronic MT group demonstrated 48% decrease compared to control group within 10 μm zone of the insertion site (Figure 8 M; *p=0.002*). Moreover, the number of iNOS and ED1 co-labeled cells was quantified. Chronic and acute MT groups showed 77% *(p<0.0001)* and 55% *(p=0.014)* reduction in M1 cells compared to control mice at the distance of 10 μm around implanted electrode, respectively (Figure 8 N), suggesting the role of MT in decreasing the pro-inflammatory responses. Interestingly, the number of the neuroprotective and regenerative M2 cells around implanted electrode in the chronic MT group yields 60% *(p=0.008)* and 46% *(p=0.019)* increase compared to control and acute MT group at 10 μm distance from implant, respectively (Figure 8 O). Additionally, the chronic MT group showed 72% increase of M2 compared to acute MT group at 10 μm-30 μm away from implant (Figure 8 O; *p=0.05*). At 30 μm-50 μm distance from insertion site in the chronic MT group, 96% *(p=0.029)* and 89% *(p=0.05)* increase of M2 were observed compared to acute MT and control group, respectively (Figure 8 O).

Furthermore, we characterized the astrocytes distribution (Figure 7 A–I). The increased expression of astrocyte (identified by glial fibrillary acidic protein, GFAP) surrounding the implanted electrode in the control was similar to what has been revealed previously [69]. Quantitatively, the chronic MT group yields almost 46% reduction in GFAP staining within 10 μm of electrode-tissue interface compared to the control group (Figure 7 J; *p=0.006*). The amount of astrocyte expression for the acute MT group was not significantly different from control ($p>0.05$), suggesting the chronic MT injection is necessary to control the persistent inflammation.

4. Discussion

Chronic reliable neural recording is important for both neuroscience research and neural prosthesis applications. However, following implantation of silicon microelectrode, there is performance degradation over time due to glial encapsulation and neuronal loss [14, 23, 26]. Typically, the deterioration in the recording quality happens over weeks and months [11, 63]. To that end, different research groups have begun investigating the key failure modes and developing strategies to improve microelectrode performance [15, 76–79]. The inflammatory response to neural implants including persistent microglia activation, glial scarring, and neuronal loss and degeneration due to the release of reactive species and pro-inflammatory molecules, are thought to be one of the failure modes [14, 76]. However, the key mediators and pathways, and the relationship between acute injury and inflammation and chronic degeneration have yet to be illustrated. There are many therapeutics targeting the inflammation and neuronal death. We chose MT because in previous studies, it was demonstrated that MT has beneficial effects against early brain injury and stroke, as well as chronic neurodegenerative diseases [40, 80, 81]. Therefore, the effects of acute and chronic MT injection on neural recording performance was investigated here with the goal of understanding biological mechanisms of recording failure and identifying key pathways to apply intervention.

4.1. Electrophysiology

4.1.1. Chronic electrochemical impedance spectroscopy—Immediately following implantation insult (the day of implantation), significant differences at 1 kHz impedance between the MT and control groups were observed (Figure 2 F) which might be related to MT pre-treatment (3 days before surgery) that has reduced the acute microglial response, the inflammatory cell infiltration and tissue swelling to the implanted electrode. In *vivo* two-photon imaging has revealed the microglia send processes immediately after implantation and these processes adhere and spread on the probes surfaces resulting in encapsulation of the devices hours after insertion [82]. Such encapsulation may partly contribute to the impedance increase. 2 photon studies will be used to further examine the effect of MT on microglia immediately after probe insertion. The impedance in all groups increased at the one-week time point following initial insertion, which is likely because of continued cellular infiltration to the implantation site and resealing of the tissue tear caused by probe insertion [83]. The impedance reaches a peak two weeks after implantation and then stabilized for all groups. This may suggest that the acute inflammation has subsided by week two and the electrode-tissue interface became stabilized from the physical barrier perspective as previously discussed [26]. Although the trend of impedance is similar among the three groups after the second week, the recording performance is significantly different ($p<0.05$), indicating that impedance is not a good predictor of neural recording [17]. More dynamic changes of the biochemical environment may have contributed to the recording quality by influencing neuronal health, viability and activity [17]. Nevertheless, it is worth pointing out that the long-term stability of the impedance from all groups suggests good mechanical and electrical stability of electrode arrays in the biological environment for the 16-week period examined.

4.1.2. Spike recording performance—We compared the evoked single-unit activity recorded from electrodes implanted in the visual cortex because this model offers more reliable neural response than spontaneous activities [26]. Furthermore, animals were anesthetized during recording to eliminate the motion artifact associated with awake recordings [84]. The results presented here demonstrated that the chronic MT treatment improves the longevity (SU yield) and quality (SU SNR, SU amplitude) of recording behavior of implanted electrodes. To investigate whether MT injection cause global increase of neural activity or increase in neuronal excitability, we compared the SU and MU firing rate at resting state and evoked MU signal to noise firing rate ratio, between different groups. No significant difference between groups over any time points were found. This suggests that the improved single unit yield by melatonin is not a result of increased activity or excitability, but more likely due to improved electrode-tissue interface (Fig. S 1).

Our data for the control group showed similar trends in recording behavior that have been reported before [11, 63]. Over the initial three weeks after insertion, the recording yield continued to drop, which corresponds to the most dynamic changes in tissue during the injury and wound healing phase. Then, the recording yield stabilized for three weeks and dropped slightly at week seven and remained low in the following weeks until the end.

During the first four weeks, implanted electrodes in the MT treated groups (acute, chronic) showed significantly higher *($p<0.05$)* SU yield, SNR, and amplitude in comparison to the control group. This improvement is likely due to the MT's effect in protecting and rescuing neurons from injury and inflammation. Interestingly, i.p. MT administration has been shown to inhibit TLR signaling pathway-related molecules such as high-mobility group box 1 (HMGB1), NF-*k*B, IL-1β, TNF-α, IL-6, and iNOS following subarachnoid hemorrhage (SAH) [80, 85]. Moreover, post-SAH or experimental diabetic neuropathy MT treatment decreases early brain injury through activating the nuclear factor E2-related factor 2 (Nrf2)-antioxidant response element (ARE) pathway and decreasing oxidative stress [81, 86]. Electrode implantation is a penetration injury and involves various degrees of bleeding. MT may have helped improve the survival of neuronal cells around recording sites in the acute to the early phase of inflammation through inhibiting similar aforementioned mechanisms.

After four weeks of implantation, the SU yield of the acute MT group dropped and showed no significant difference from the control group suggesting that inflammatory and/or reactive species continue to be produced near the chronic implants, and acute use of MT is not enough to maintain a long-term electrode-tissue interface. On the contrary, the chronically treated MT group maintained significantly higher SU yield compared to both the acute MT (week 5–16) and control (week 0–16) mice (Figure 2 A), highlighting the necessity of MT administration throughout the chronic implantation.

Previous studies have showed persistent presence of activated microglia/macrophage at the vicinity of the implants [23]. These cells release pro-inflammatory cytokines that may trigger the neuronal death. Furthermore, continuous blood brain barrier leakage has been reported which may further exacerbate inflammation and cause neuronal loss and demyelination. The triggers of these ongoing inflammation might be mechanical mismatch between the implants and the brain tissue, micromotion, incomplete sealing of the BBB or toxic leachables [15, 87]. Recent reports show that there are several pathways that MT may utilize to prevent chronic neuronal loss. First, MT may counteract inflammatory processes by regulating both pro- and anti-inflammatory cytokines [29, 88, 89] and control microglia behavior [90, 91]. Secondly, it is known that reactive oxygen and nitrogen species released by microglia/macrophages are harmful to neurons, trigger inflammation and BBB breach, which in turn further cause neuron and myelin degeneration. MT can reduce oxidative stress by either directly scavenging free radicals produced by activated microglia [92], or activating antioxidant enzymes [30, 93, 94]. Thirdly, in general, MT is highly protective to cells under severe inflammatory conditions [29, 39]. MT exerts neuroprotective effect by suppressing neutrophil infiltration [88] and inhibiting TNF-α toxicity which may be due to reduction of Ca^{2+} influx and activation of caspase-3 following oxidative stress [95]. In summary, MT may improve recording performance via some or all of the following actions: anti-inflammatory, anti-apoptotic and antioxidant. Histological analysis offers further insights in these biological mechanisms.

4.2. Histology

Although, previous studies have quantified the tissue response to chronically-implanted intracortical microelectrodes, correlations between various tissue markers and recording

performance over time remain largely unclear and cannot be generalized [17, 26, 96]. As such, the most impactful cellular pathways leading to recording failure has yet to be identified. We observed significant improvement by MT treatment on neural recording, as well as significant difference between the acute and chronic drug administrations. This offers a great opportunity to pinpoint the biological factors that play significant roles in recording quality by combining recording data with comprehensive histological analysis. Immunohistochemical analysis conducted below aimed at investigating how MT administration has improved the quality and longevity of chronic neural implants, via its anti-apoptotic, antioxidant or anti-inflammatory effects.

4.2.1. Effect of daily MT administration on neurodegeneration—It is suggested that density and viability of neuronal cells around the insertion site directly effects the recording quality [76] and the first 50 μm of implanted electrodes is crucial for optimal device function [97]. Notably, our quantitative results of caspase-3 and NeuN staining at week 16, showed fewer caspase-3 positive neurons in the chronic MT group compared to control at 10 μm from the implant (Figure 4 K) and more viable neuronal cells in the chronic MT group than the acute MT and control groups in 30 μm zone around the interface (Figure 4 J). These results correspond well to the recording outcomes. Also, we noted that administration of MT at 30 mg/kg/day for only 14 days did not result in any significant improvement on neuronal cell density and health around the implanted electrode at week 16 (Figure 4 J), suggesting that neuronal damage continued to occur past the acute administration period and chronic MT administration is necessary and effective in maintaining neuronal density and health over the entire implantation period. A previous study showed that i.p injection of MT 30 mg/kg inhibits caspase-1/cytochrome *c*/caspase-3 cell death pathway in transgenic amyotrophic lateral sclerosis (ALS) mice [40]. The MT treatment in our study might have rescued neurons following similar mechanisms.

4.2.2. Effect of daily MT administration on oxidative stress—Several studies have reported an antioxidant role of MT in scavenging free radicals and inhibiting inflammatory processes [34, 93, 98]. Recently, it was declared that long-term oral MT treatment (10 mg/kg/day) has reduced the oxidative stress and inflammation in the aortas of aging mice [99]. 4-hydroxynonenal (4-HNE), a product of lipid peroxidation, is a commonly used biomarker for oxidative stress. MT has inhibitory effects on lipid peroxidation by ROS and is known as a cell membrane protector [39]. Notably, we found significant higher level of 4HNE staining within 30 μm zone of the implants in the control group, providing a strong evidence of high oxidative stress around the implants (Figure 5 G). This effect is highly localized to within the 30 μm of the implant and correlated to the reduction of NeuN positive cells in this region. Meanwhile, significant reduction of 4HNE around implanted electrodes in the chronic MT group was found compared to the control (from 0 to 30 μm distance), while the acute MT did not yield the same improvement at 16 weeks post implantation (Figure 5 G). This finding is consistent with higher single-unit yield in the chronic MT group compared to the acute MT and control group. Previous studies have hypothesized minimizing oxidative stress can improve neural interface performance [18, 79], because free radicals can cause degradation of passivation layers and insulating coatings [100, 101], degeneration of neuronal cells [102] and increase of pro-inflammatory molecules via NF-KB

signaling pathway [103]. Notably, we did not observe material failure based on the stable impedance in all groups for the 16 weeks examined. However, we did find a strong correlation between high level of ROS and loss of neurons, and showed that application of MT effectively maintained neuronal density and neural recording.

4.2.3. Effect of daily MT administration on BBB stability—Electrode insertion inevitably damages the BBB, which could lead to acute inflammation and neuronal loss [104]. Chronically, BBB permeability may continue to be compromised by the presence of implants due to movement, mechanical mismatch or release of inflammatory stimuli such as ROS or cytokines [14]. BBB breakdown at the electrode-brain tissue interface has been suggested to affect neuronal viability [105]. Recently, it was reported that BBB leakage was correlated to local accumulation of neurotoxic factors such as IL-1β and TNF-α that lead to neuronal death, which directly affect neuronal signal quality [106]. Beyond directly impacting signal quality, infiltrating blood products, like extravasated fibrinogen, cause a persistent neuroinflammation (macrophage and microglial activation) around the implant [76]. Following extravasation, blood-products activate inflammatory cell through TLR pathway [76]. Recently, it was suggested that i.p. injection of 15 mg/kg/day of MT for one week, inhibited BBB leakage by preventing the TLR4/NFKB signaling pathway in neonatal rats [107]. Therefore, we hypothesized MT administration may improve recording quality by inhibiting the BBB disruption and improving neuronal survival at the electrode tissue interface. Our results following daily administration of MT for either short-term or long-term treatment were promising and both MT groups had significantly lower IgG staining than control animals up to 30 μm (acute MT) and 10 μm away from the implant interface (Figure 6 J, Fig. S 2). This result suggests that for single shank NeuroNexus planar probes, BBB leakage can be reduced and perhaps healed by even acute MT treatment. However, reduced IgG staining in the acute MT group did not lead to improved neuronal health and recording quality at the later stage. Therefore, IgG staining is not a good predictor of recording quality. Tomato lectin is an endothelial marker for imaging vasculature structures in the central nervous system [108, 109]. In addition to vasculature, it can also visualize amoeboid microglia in the developing brain, ramified microglia in the adult, and activated/reactive microglia in the experimentally damaged brain [71, 110] and allowing to study the relationship between microglial cells and vasculature [71]. Our tomato lectin staining (Figure 7 D–F) showed uniform distribution of capillaries in the image field in all three groups. However, at the vicinity of the probe, an enhanced staining was found in the control group, primarily due to the increased microglia/macrophage presence at the injury site. Both acute and chronic MT treatment demonstrated significant reduction of lectin intensity compared to control suggesting that acute MT treatment is sufficient to subside majority of the microglia activation (Figure 7 K).

4.2.4. Effect of daily MT administration on inflammatory gliosis—Activation of microglia is a key factor in the inflammatory response to injury [111]. Activated microglia produce cytotoxic molecules such as nitric oxide and cytokines which can cause secondary neuronal damage [90]. The i.p. injection of MT 0–4 hours after TBI, has markedly restrained microglial activation and reduced protein expression of pro-inflammatory cytokines like IL-1ß and TNF-α [90]. Also, MT has been shown to inhibit microglia activation in hypoxia/

ischemic brain damage [80]. Some results have emphasized the importance of the therapeutic time-window after the initial injury in TBI [112]. Our results showed that MT delivery in both acute and chronic schedule has significantly decreased microglia activation compared to control based on lectin and Iba-1 staining in Figure 7 K, and Figure 6 K, respectively. This data suggest that acute MT treatment would be sufficient in attenuating microglia activation. However, upon activation, microglia may adopt different phenotypes and perform different function. M1 macrophages are pro-inflammation and cause neurotoxicity and axonal death, while M2 macrophages promote axonal growth and re-myelination [73, 113, 114]. Previous studies demonstrated that MT modulates both pro- and anti-inflammatory cytokines in different pathophysiological conditions [29, 115]. To better evaluate the MT's action on microglia at the implantation site, we used markers of M1 (iNOS) and M2 (Arg1) with co-label of ED-1 (all activated microphage/microglia) and showed that the density of M1 macrophages in both acute and chronic MT treatment schedule was lower than control only within the 10 μm zone of the electrode tissue interface (Figure 8 N); however, the density of M2 macrophages was higher in chronic MT group compared to acute MT and control throughout the 50 μm zone of the insertion site (Figure 8 O). This suggests that Iba-1 or ED-1 intensity alone is not sufficient to characterize the inflammatory response and consequently these markers may not be good indicators to predict recording outcomes. Higher amount of M2 cells as the result of chronic MT treatment may have promoted the regeneration and healing of the neural tissue, which leads to the ultimate stable long-term recording. Additional analysis quantifying the pro- and anti-inflammatory cytokines should reveal the microglia action in more detail.

GFAP labels reactive astrocyte and is a good indicator of gliosis in response to neural damage. It was shown that m T treatment reduced GFAP expression in all brain regions of diabetic rats [116] and ischemic mouse retina [117]. Also, the protective role of MT in attenuating glial activation in response to domoic acid-induced neuronal damage was reported [118]. Figure 7 J showed significantly less glial encapsulation around implanted electrode in the chronic MT treated group than control 10 μm away from the insertion site. This data correlates with higher signal to noise ratio in the chronic MT group. On the other hand, the acute MT group showed no statistically significant difference in GFAP intensity from the control. This suggests that MT treatment has decreased the initial glial activation, however due to persistent inflammation, the acute treatment of MT was not sufficient and it was necessary to continue MT administration to attenuate gliosis.

4.2.5. Depth Dependence of Tissue Responses—Furthermore, we have run additional staining and imaging to examine the more superficial depth (0–500um) and the deep regions (1000–1500 um). The intensity analysis for IgG, lectin, Iba-1 and GFAP all three depth regions are shown in supplementary figures as Fig. S 2 and Fig. S 3. In the top region, we observed statistically significant lower IgG expression in the chronic MT treated group compared to the control, which corresponds well to the higher recorded single unit yield observed in the heat map (Figure 3). Moreover, significantly lower GFAP and Iba-1 intensity in both MT treated groups were observed in comparison to the control (Fig. S 3 A and Fig. S 2 D). At the deeper region, there were significantly lower GFAP and Iba-1 signal intensities in chronic MT group compared to the control within the 10 μm zone of the

implant (Fig. S 3 C and Fig. S 2 F), which correlates well to the higher recording yield in the chronic MT in this depth. The acute MT treatment did not show any significant difference compared to the control for Iba-1 and GFAP expression in the deeper region and for IgG in the top region of the brain though. In addition, trending decreases of IgG (Fig. S 2 C) and lectin (Fig. S 3 F) signals within the first 10 μm bin in the chronic MT group were observed compared to the saline, but these are not statistically significant.

4.2.6. Discussion on drug dosage and schedule and potential use in human

—Due to the short-half-life of MT (less than one hour) [119], fresh preparation of MT for injection is the most effective method for inhibiting the inflammation. Therefore, immediately after drug preparation, i.p. injections were performed. Also, according to the previous reports [18, 22], it was hypothesized that three days treatment before surgery may be beneficial to decrease the strength of initial tissue response to the implanted electrode. Our results indicated that MT improved SNR and SU yield at the day of surgery compared to the control group and this improvement may be related to the MT pre-treatment. Later, we noted that recording quality became stable even in the control group after 7 weeks, so shorter chronic dosing regimens (for 7 weeks) could be performed to determine the optimized injection schedule.

Several studies have examined the effects of anti-inflammatory and/or neuroprotective drugs on neural tissue reaction to implanted electrodes [18, 22, 120, 121]. However, fewer studies reported improvement over recording quality and longevity upon these treatments [22]. Among these, minocycline has been administrated orally (dissolved in water) 2 days prior and 5 days after implantation surgery in rats. Improved recording was reported up to 4 weeks with decreased astrocyte activity [22]. Since the study ended at 4 weeks, the longer-term effect of the acute minocycline treatment is unknown. Others studied the effect of naturally derived anti-oxidants, such as resveratrol, in providing neuroprotection around neural electrodes by mediating the expression of anti-oxidative enzymes [120]. The acute resveratrol treated animals (16–24 h before surgery) resulted in lower amount of free radicals than the controls, two weeks post-implant. However, this dosing regimen did not inhibit the glial scar around the implanted electrode [120]. In a follow-up study, i.p. daily injection of resveratrol at 200 mg/kg for 16 weeks resulted in better neuronal survival and reduced superoxide level around the neural probes [18], which is consistent with the effects observed in our chronic MT treatment. However, no recording was performed in this resveratrol study, so the effect of resveratrol on recording quality and longevity has yet to be demonstrated.

Intraperitoneal daily injection of resveratrol resulted in increasing the BBB leakage at 2 weeks, which recovered to the same level as the control at 16 weeks [18]. On the contrary, we observed reduced IgG staining from control at 16 weeks suggesting a BBB stabilizing effect from the MT. Finally, increased hemorrhaging in the liver and thread-like adhesions between the liver and diaphragm was noted at sixteen weeks, as secondary side effect of resveratrol or repeated i.p. injection [18]. Oral administration was also tested in this study, but the concentration in the brain was undetectable. Low bioavailability of resveratrol has been a major challenge for use of this antioxidant in humans [122], and advanced delivery techniques are needed to achieve effective concentration in the targeted brain area without

unwanted side effect to the peripheries [123]. Remarkably, oral MT treatment (1 to 300 mg) or daily administration of 1 g MT for 30 days had no side effects in humans [124], making MT a promising therapy for human applications. Although short-term usage (3 months or less) of melatonin appears to be safe [124–126], the safety for extended use is not clear due to lack of studies. Recently, Posadzki et al reviewed the health outcome and adverse effects reported for melatonin in clinically heterogeneous populations. These adverse effects include morning drowsiness, vivid dream, headaches, dizziness, gastro-intestinal symptoms and worsening of seizures and asthma. This review calls for more high quality randomized clinical trials for decreasing the uncertainties [127]. Meanwhile, several studies suggest that long-term melatonin uses have the potential for treating chronic disease [54, 128]. Nevertheless, continuous systemic MT administration may not be the ideal solution and localized controlled delivery strategies should be developed.

5. Conclusions

The results of this study provide evidence of MT's potent effect in improving the chronic intracortical recording performance of the electrode. In summary, chronic MT delivery maintains a high single-unit yield over 16 weeks of study. Acute MT delivery improves the early recording performance but the effect fades completely 2 weeks after the injection stopped. Histological studies revealed a significant increase in neuronal viability and reduction in neuronal apoptosis around implanted electrode at week 16 in the chronic MT group in comparison to control and acute MT treated subjects, which is correlated with reduced oxidative stress and increased expression of neuro-regenerative Arg-1. This result suggests that MT promotes neuroprotection possibly through anti-apoptotic, anti-inflammatory signaling and antioxidative properties. Additional studies are necessary to further dissect the mechanism of action of MT by examining the role of MT receptors. It can be concluded that continuous MT injection may be a viable solution for improving long-term recording quality, while the development of sustained local MT delivery techniques are warranted.

Supplementary Material

Refer to Web version on PubMed Central for supplementary material.

Acknowledgments:

The authors like to thank Jin-Ho Kim for helpful discussion on ROS staining. The authors thank the center for Biological Imaging at the University of Pittsburgh for confocal microscopy.

Funding: This work was supported by the National Institute of Health [grant numbers R01NS089688, R01NS094396 and R01NS062019).

References:

[1]. Hatsopoulos NG, Donoghue JP. The science of neural interface systems. Annu Rev Neurosci 2009;32:249–66. [PubMed: 19400719]

[2]. Schwartz AB, Cui XT, Weber DJ, Moran DW. Brain-controlled interfaces: movement restoration with neural prosthetics. Neuron. 2006;52:205–20. [PubMed: 17015237]

[3]. Kipke DR, Shain W, Buzsaki G, Fetz E, Henderson JM, Hetke JF, et al. Advanced neurotechnologies for chronic neural interfaces: new horizons and clinical opportunities. Journal of Neuroscience. 2008;28:11830–8. [PubMed: 19005048]

[4]. Buzsaki G, Stark E, Berenyi A, Khodagholy D, Kipke DR, Yoon E, et al. Tools for probing local circuits: high-density silicon probes combined with optogenetics. Neuron. 2015;86:92–105. [PubMed: 25856489]

[5]. Berényi A, Somogyvári Z, Nagy AJ, Roux L, Long JD, Fujisawa S, et al. Large-scale, high-density (up to 512 channels) recording of local circuits in behaving animals. Journal of Neurophysiology. 2014;111:1132–49. [PubMed: 24353300]

[6]. Hochberg LR, Serruya MD, Friehs GM, Mukand JA, Saleh M, Caplan AH, et al. Neuronal ensemble control of prosthetic devices by a human with tetraplegia. Nature. 2006;442:164–71. [PubMed: 16838014]

[7]. Collinger JL, Wodlinger B, Downey JE, Wang W, Tyler-Kabara EC, Weber DJ, et al. High-performance neuroprosthetic control by an individual with tetraplegia. Lancet. 2013;381:557–64. [PubMed: 23253623]

[8]. Flesher SN, Collinger JL, Foldes ST, Weiss JM, Downey JE, Tyler-Kabara EC, et al. Intracortical microstimulation of human somatosensory cortex. Science Translational Medicine. 2016.

[9]. Chestek CA, Gilja V, Nuyujukian P, Foster JD, Fan JM, Kaufman MT, et al. Long-term stability of neural prosthetic control signals from silicon cortical arrays in rhesus macaque motor cortex. J Neural Eng 2011;8:045005. [PubMed: 21775782]

[10]. Schwartz AB. Cortical neural prosthetics. Annual Review of Neuroscience. 2004;27:487–507.

[11]. Nicolelis MAL, Dimitrov D, Carmena JM, Crist R, Lehew G, Kralik JD, et al. Chronic, multisite, multielectrode recordings in macaque monkeys. PNAS. 2003;100:11041–6. [PubMed: 12960378]

[12]. Rousche PJ, Normann RA. Chronic recording capability of the Utah Intracortical Electrode Array in cat sensory cortex. J Neurosci Methods. 1998;82:1–15. [PubMed: 10223510]

[13]. Prasad A, Sankar V, Dyer AT, Knott E, Xue QS, Nishida T, et al. Coupling biotic and abiotic metrics to create a testbed for predicting neural electrode performance. Conf Proc IEEE Eng Med Biol Soc 2011;2011:3020–3. [PubMed: 22254976]

[14]. Kozai TD, Jaquins-Gerstl AS, Vazquez AL, Michael AC, Cui XT. Brain tissue responses to neural implants impact signal sensitivity and intervention strategies. Acs Chem Neurosci. 2015;6:48–67. [PubMed: 25546652]

[15]. Wellman SM, Eles JR, Ludwig KA, Seymour JP, Michelson NJ, McFadden WE, et al. A Materials Roadmap to Functional Neural Interface Design. Advanced Functional Materials. 2017.

[16]. Salatino JW, Winter BM, Drazin MH, Purcell EK. Functional Remodeling of Subtype-Specific Markers Surrounding Implanted Neuroprostheses. J Neurophysiol 2017:jn 00162 2017.

[17]. Michelson NJ, Vazquez AL, Eles JR, Salatino JW, Purcell EK, Williams JJ, et al. Multi-scale, multi-modal analysis uncovers complex relationship at the brain tissue-implant neural interface: New Emphasis on the Biological Interface. Journal of Neural Engineering. 2017.

[18]. Potter-Baker KA, Stewart WG, Tomaszewski WH, Wong CT, Meador WD, Ziats NP, et al. Implications of chronic daily anti-oxidant administration on the inflammatory response to intracortical microelectrodes. J Neural Eng 2015;12:046002. [PubMed: 26015427]

[19]. Polikov VS, Tresco PA, Reichert WM. Response of brain tissue to chronically implanted neural electrodes. J Neurosci Methods. 2005;148:1–18. [PubMed: 16198003]

[20]. Wellman SM, Kozai TDY. In vivo spatiotemporal dynamics of NG2 glia activity caused by neural electrode implantation. Biomaterials. 2018.

[21]. Wellman SM, Kozai TDY. Understanding the Inflammatory Tissue Reaction to Brain Implants To Improve Neurochemical Sensing Performance. ACS Chemical Neuroscience. 2017.

[22]. Rennaker RL, Miller J, Tang H, Wilson DA. Minocycline increases quality and longevity of chronic neural recordings. J Neural Eng 2007;4:L1–5. [PubMed: 17409469]

[23]. Biran R, Martin DC, Tresco PA. Neuronal cell loss accompanies the brain tissue response to chronically implanted silicon microelectrode arrays. Experimental Neurology. 2005;195:115–26. [PubMed: 16045910]

[24]. Szarowski DH, Andersen MD, Retterer S, Spence AJ, Isaacson M, Craighead HG, et al. Brain responses to micro-machined silicon devices. Brain Res 2003;983:23–35. [PubMed: 12914963]

[25]. Sohal HS, Jackson A, Jackson R, Clowry GJ, Vassilevski K, O'Neill A, et al. The sinusoidal probe: a new approach to improve electrode longevity. Frontiers in Neuroengineering. 2014;7:10. [PubMed: 24808859]

[26]. Kozai TD, Li X, Bodily LM, Caparosa EM, Zenonos GA, Carlisle DL, et al. Effects of caspase-1 knockout on chronic neural recording quality and longevity: insight into cellular and molecular mechanisms of the reactive tissue response. Biomaterials. 2014;35:9620–34. [PubMed: 25176060]

[27]. McConnell GC, Rees HD, Levey AI, Gutekunst CA, Gross RE, Bellamkonda RV. Implanted neural electrodes cause chronic, local inflammation that is correlated with local neurodegeneration. J Neural Eng 2009;6:056003. [PubMed: 19700815]

[28]. Hermann JK, Ravikumar M, Shoffstall A, Ereifej ES, Kovach K, Chang J, et al. Inhibition of the cluster of differentiation 14 innate immunity pathway with IAXO-101 improves chronic microelectrode performance. J Neural Eng 2017.

[29]. Mauriz JL, Collado PS, Veneroso C, Reiter RJ, Gonzalez-Gallego J. A review of the molecular aspects of melatonin's anti-inflammatory actions: recent insights and new perspectives. J Pineal Res 2013;54:1–14. [PubMed: 22725668]

[30]. Favero G, Franceschetti L, Bonomini F, Rodella LF, Rezzani R. Melatonin as an Anti-Inflammatory Agent Modulating Inflammasome Activation. International Journal of Endocrinology. 2017;2017:13.

[31]. Lin C, Chao H, Li Z, Xu X, Liu Y, Hou L, et al. Melatonin attenuates traumatic brain injury-induced inflammation: a possible role for mitophagy. J Pineal Res 2016;61:177–86. [PubMed: 27117839]

[32]. Zhang H-M, Zhang Y. Melatonin: a well-documented antioxidant with conditional pro-oxidant actions. Journal of Pineal Research. 2014;57:131–46. [PubMed: 25060102]

[33]. Manchester LC, Coto-Montes A, Boga JA, Andersen LP, Zhou Z, Galano A, et al. Melatonin: an ancient molecule that makes oxygen metabolically tolerable. J Pineal Res 2015;59:403–19. [PubMed: 26272235]

[34]. Tan DX, Manchester LC, Esteban-Zubero E, Zhou Z, Reiter RJ. Melatonin as a Potent and Inducible Endogenous Antioxidant: Synthesis and Metabolism. Molecules. 2015;20:18886–906. [PubMed: 26501252]

[35]. Bizzarri M, Proietti S, Cucina A, Reiter RJ. Molecular mechanisms of the pro-apoptotic actions of melatonin in cancer: a review. Expert opinion on therapeutic targets. 2013;17:1483–96. [PubMed: 24032643]

[36]. Carrillo-Vico A, Lardone PJ, Alvarez-Sanchez N, Rodriguez-Rodriguez A, Guerrero JM. Melatonin: buffering the immune system. Int J Mol Sci 2013;14:8638–83. [PubMed: 23609496]

[37]. Radogna F, Diederich M, Ghibelli L. Melatonin: A pleiotropic molecule regulating inflammation. Biochemical Pharmacology. 2010;80:1844–52. [PubMed: 20696138]

[38]. Eghbal MA EA, Ahmadian E, Azarmi Y, Parvizpur A. A Review of Biological and Pharmacological Actions of Melatonin: Oxidant and Prooxidant Properties. Pharmacological Reports. 2016;1:9.

[39]. Esposito E, Cuzzocrea S. Antiinflammatory Activity of Melatonin in Central Nervous System. Current neuropharmacology. 2010;8:228–42. [PubMed: 21358973]

[40]. Zhang Y, Cook A, Kim J, Baranov SV, Jiang J, Smith K, et al. Melatonin inhibits the caspase-1/cytochrome c/caspase-3 cell death pathway, inhibits MT1 receptor loss and delays disease progression in a mouse model of amyotrophic lateral sclerosis. Neurobiology of disease. 2013;55:26–35. [PubMed: 23537713]

[41]. Suofu Y, Li W, Jean-Alphonse FG, Jia J, Khattar NK, Li J, et al. Dual role of mitochondria in producing melatonin and driving GPCR signaling to block cytochrome c release. Proc Natl Acad Sci U S A. 2017;114:E7997–E8006. [PubMed: 28874589]

[42]. Jou MJ, Peng TI, Hsu LF, Jou SB, Reiter RJ, Yang CM, et al. Visualization of melatonin's multiple mitochondrial levels of protection against mitochondrial Ca(2+)-mediated permeability transition and beyond in rat brain astrocytes. J Pineal Res 2010;48:20–38. [PubMed: 19925580]

[43]. Paradies G, Petrosillo G, Paradies V, Reiter RJ, Ruggiero FM. Melatonin, cardiolipin and mitochondrial bioenergetics in health and disease. J Pineal Res 2010;48:297–310. [PubMed: 20433638]

[44]. Sainz RM, Mayo JC, Rodriguez C, Tan DX, Lopez-Burillo S, Reiter RJ. Melatonin and cell death: differential actions on apoptosis in normal and cancer cells. Cellular and Molecular Life Sciences CMLS. 2003;60:1407–26. [PubMed: 12943228]

[45]. Pappolla MA, Sos M, Omar RA, Bick RJ, Hickson-Bick DL, Reiter RJ, et al. Melatonin prevents death of neuroblastoma cells exposed to the Alzheimer amyloid peptide. The Journal of neuroscience : the official journal of the Society for Neuroscience. 1997;17:1683–90. [PubMed: 9030627]

[46]. Sainz RM, Mayo JC, Uria H, Kotler M, Antolin I, Rodriguez C, et al. The pineal neurohormone melatonin prevents in vivo and in vitro apoptosis in thymocytes. J Pineal Res 1995;19:178–88. [PubMed: 8789249]

[47]. Deigner HP, Haberkorn U, Kinscherf R. Apoptosis modulators in the therapy of neurodegenerative diseases. Expert opinion on investigational drugs. 2000;9:747–64. [PubMed: 11060707]

[48]. Brewer GJ. Neuronal plasticity and stressor toxicity during aging. Experimental Gerontology. 2000;35:1165–83. [PubMed: 11113600]

[49]. Agil A, Reiter RJ, Jimenez-Aranda A, Iban-Arias R, Navarro-Alarcon M, Marchal JA, et al. Melatonin ameliorates low-grade inflammation and oxidative stress in young Zucker diabetic fatty rats. J Pineal Res 2013;54:381–8. [PubMed: 23020082]

[50]. Tsai MC, Chen WJ, Tsai MS, Ching CH, Chuang JI. Melatonin attenuates brain contusion-induced oxidative insult, inactivation of signal transducers and activators of transcription 1, and upregulation of suppressor of cytokine signaling-3 in rats. J Pineal Res 2011;51:233–45. [PubMed: 21545521]

[51]. Lin XJ, Mei GP, Liu J, Li YL, Zuo D, Liu SJ, et al. Therapeutic effects of melatonin on heatstroke-induced multiple organ dysfunction syndrome in rats. J Pineal Res 2011;50:436–44. [PubMed: 21392091]

[52]. Veneroso C, Tunon MJ, Gonzalez-Gallego J, Collado PS. Melatonin reduces cardiac inflammatory injury induced by acute exercise. J Pineal Res 2009;47:184–91. [PubMed: 19627457]

[53]. Deng WG, Tang ST, Tseng HP, Wu KK. Melatonin suppresses macrophage cyclooxygenase-2 and inducible nitric oxide synthase expression by inhibiting p52 acetylation and binding. Blood. 2006;108:518–24. [PubMed: 16609073]

[54]. Korkmaz A, Reiter RJ, Topal T, Manchester LC, Oter S, Tan DX. Melatonin: an established antioxidant worthy of use in clinical trials. Molecular medicine. 2009;15:43–50. [PubMed: 19011689]

[55]. Permpoonputtana K, Govitrapong P. The anti-inflammatory effect of melatonin on methamphetamine-induced proinflammatory mediators in human neuroblastoma dopamine SH-SY5Y cell lines. Neurotoxicity research. 2013;23:189–99. [PubMed: 22903344]

[56]. Bruck R, Aeed H, Avni Y, Shirin H, Matas Z, Shahmurov M, et al. Melatonin inhibits nuclear factor kappa B activation and oxidative stress and protects against thioacetamide induced liver damage in rats. Journal of hepatology. 2004;40:86–93. [PubMed: 14672618]

[57]. Yoo Y-M, Yim S-V, Kim S-S, Jang HY, Lea HZ, Hwang G-C, et al. Melatonin suppresses NO-induced apoptosis via induction of Bcl-2 expression in PGT-P immortalized pineal cells. Journal of Pineal Research. 2002;33:146–50. [PubMed: 12220328]

[58]. Vriend J, Reiter RJ. Melatonin as a proteasome inhibitor. Is there any clinical evidence? Life sciences. 2014;115:8–14. [PubMed: 25219883]

[59]. Kleiner M, Brainard D, Pelli D, Ingling A, Murray R, Broussard C. What's new in Psychtoolbox-3. Perception. 2007;36:1.

[60]. Brainard DH. The psychophysics toolbox. Spatial vision. 1997;10:433–6. [PubMed: 9176952]

[61]. Cornelissen FW, Peters EM, Palmer J. The Eyelink Toolbox: eye tracking with MATLAB and the Psychophysics Toolbox. Behavior Research Methods. 2002;34:613–7.

[62]. Kozai TDY, Langhals NB, Patel PR, Deng X, Zhang H, Smith KL, et al. Ultrasmall implantable composite microelectrodes with bioactive surfaces for chronic neural interfaces. Nature materials. 2012;11:1065–73. [PubMed: 23142839]

[63]. Kozai TD, Du Z, Gugel ZV, Smith MA, Chase SM, Bodily LM, et al. Comprehensive chronic laminar single-unit, multi-unit, and local field potential recording performance with planar single shank electrode arrays. J Neurosci Methods. 2015;242:15–40. [PubMed: 25542351]

[64]. Zhang Y, Cook A, Kim JH, Baranov SV, Jiang JY, Smith K, et al. Melatonin inhibits the caspase-1/cytochrome c/caspase-3 cell death pathway, inhibits MT1 receptor loss and delays disease progression in a mouse model of amyotrophic lateral sclerosis. Neurobiology of Disease. 2013;55:26–35. [PubMed: 23537713]

[65]. Pelli DG. The VideoToolbox software for visual psychophysics: Transforming numbers into movies. Spatial vision. 1997;10:437–42. [PubMed: 9176953]

[66]. Ludwig KA, Miriani RM, Langhals NB, Joseph MD, Anderson DJ, Kipke DR. Using a common average reference to improve cortical neuron recordings from microelectrode arrays. Journal of neurophysiology. 2009;101:1679–89. [PubMed: 19109453]

[67]. Wagenaar DA, Potter SM. Real-time multi-channel stimulus artifact suppression by local curve fitting. Journal of neuroscience methods. 2002;120:113–20. [PubMed: 12385761]

[68]. Fee MS, Mitra PP, Kleinfeld D. Automatic sorting of multiple unit neuronal signals in the presence of anisotropic and non-Gaussian variability. Journal of Neuroscience Methods. 1996;69:175–88. [PubMed: 8946321]

[69]. Kozai TDY, Gugel Z, Li X, Gilgunn PJ, Khilwani R, Ozdoganlar OB, et al. Chronic tissue response to carboxymethyl cellulose based dissolvable insertion needle for ultra-small neural probes. Biomaterials. 2014;35:9255–68. [PubMed: 25128375]

[70]. Potter KA, Buck AC, Self WK, Capadona JR. Stab injury and device implantation within the brain results in inversely multiphasic neuroinflammatory and neurodegenerative responses. J Neural Eng 2012;9:046020. [PubMed: 22832283]

[71]. Villacampa N, Almolda B, Gonzalez B, Castellano B. Tomato Lectin Histochemistry for Microglial Visualization In: Joseph B, Venero JL, editors. Microglia: Methods and Protocols. Totowa, NJ: Humana Press; 2013 p. 261–79.

[72]. Robertson RT, Levine ST, Haynes SM, Gutierrez P, Baratta JL, Tan Z, et al. Use of labeled tomato lectin for imaging vasculature structures. Histochemistry and cell biology. 2015;143:225–34. [PubMed: 25534591]

[73]. Gensel JC, Kopper TJ, Zhang B, Orr MB, Bailey WM. Predictive screening of M1 and M2 macrophages reveals the immunomodulatory effectiveness of post spinal cord injury azithromycin treatment. Scientific reports. 2017;7:40144. [PubMed: 28057928]

[74]. Martinez FO, Gordon S. The M1 and M2 paradigm of macrophage activation: time for reassessment. F1000Prime Reports. 2014;6:13. [PubMed: 24669294]

[75]. Dijkstra CD, Dopp EA, Joling P, Kraal G. The heterogeneity of mononuclear phagocytes in lymphoid organs: distinct macrophage subpopulations in the rat recognized by monoclonal antibodies ED1, ED2 and ED3. Immunology. 1985;54:589–99. [PubMed: 3882559]

[76]. Jorfi M, Skousen JL, Weder C, Capadona JR. Progress towards biocompatible intracortical microelectrodes for neural interfacing applications. J Neural Eng 2015;12:011001. [PubMed: 25460808]

[77]. Kozai TD, Catt K, Li X, Gugel ZV, Olafsson VT, Vazquez AL, et al. Mechanical failure modes of chronically implanted planar silicon-based neural probes for laminar recording. Biomaterials. 2015;37:25–39. [PubMed: 25453935]

[78]. Barrese JC, Rao N, Paroo K, Triebwasser C, Vargas-Irwin C, Franquemont L, et al. Failure mode analysis of silicon-based intracortical microelectrode arrays in non-human primates. Journal of Neural Engineering. 2013;10:066014. [PubMed: 24216311]

[79]. Prasad A, Xue Q-S, Dieme R, Sankar V, Mayrand RC, Nishida T, et al. Abiotic-biotic characterization of Pt/Ir microelectrode arrays in chronic implants. Frontiers in Neuroengineering. 2014;7:2. [PubMed: 24550823]

[80]. Wang Z, Wu L, You W, Ji C, Chen G. Melatonin alleviates secondary brain damage and neurobehavioral dysfunction after experimental subarachnoid hemorrhage: possible involvement

of TLR4-mediated inflammatory pathway. Journal of Pineal Research. 2013;55:399–408. [PubMed: 24007200]

[81]. Wang Z, Ma C, Meng CJ, Zhu GQ, Sun XB, Huo L, et al. Melatonin activates the Nrf2-ARE pathway when it protects against early brain injury in a subarachnoid hemorrhage model. J Pineal Res 2012;53:129–37. [PubMed: 22304528]

[82]. Kozai TD, Vazquez AL, Weaver CL, Kim SG, Cui XT. In vivo two-photon microscopy reveals immediate microglial reaction to implantation of microelectrode through extension of processes. J Neural Eng 2012;9:066001. [PubMed: 23075490]

[83]. Purcell EK, Thompson DE, Ludwig KA, Kipke DR. Flavopiridol reduces the impedance of neural prostheses in vivo without affecting recording quality. J Neurosci Methods. 2009;183:149–57. [PubMed: 19560490]

[84]. Michelson NJ, Vazquez AL, Eles JR, Salatino JW, Purcell EK, Williams JJ, et al. Multi-scale, multi-modal analysis uncovers complex relationship at the brain tissue-implant neural interface: New Emphasis on the Biological Interface. J Neural Eng 2017.

[85]. Kang J-W, Koh E-J, Lee S-M. Melatonin protects liver against ischemia and reperfusion injury through inhibition of toll-like receptor signaling pathway. Journal of Pineal Research. 2011;50:403–11. [PubMed: 21355876]

[86]. Negi G, Kumar A, Sharma SS. Melatonin modulates neuroinflammation and oxidative stress in experimental diabetic neuropathy: effects on NF-kappaB and Nrf2 cascades. J Pineal Res 2011;50:124–31. [PubMed: 21062351]

[87]. Subbaroyan J, Martin DC, Kipke DR. A finite-element model of the mechanical effects of implantable microelectrodes in the cerebral cortex. J Neural Eng 2005;2:103–13. [PubMed: 16317234]

[88]. Pazar A, Kolgazi M, Memisoglu A, Bahadir E, Sirvanci S, Yaman A, et al. The neuroprotective and anti-apoptotic effects of melatonin on hemolytic hyperbilirubinemia-induced oxidative brain damage. J Pineal Res 2016;60:74–83. [PubMed: 26511903]

[89]. Liu X, Gong Y, Xiong K, Ye Y, Xiong Y, Zhuang Z, et al. Melatonin mediates protective effects on inflammatory response induced by interleukin-1 beta in human mesenchymal stem cells. Journal of Pineal Research. 2013;55:14–25. [PubMed: 23488678]

[90]. Ding K, Wang H, Xu J, Lu X, Zhang L, Zhu L. Melatonin reduced microglial activation and alleviated neuroinflammation induced neuron degeneration in experimental traumatic brain injury: Possible involvement of mTOR pathway. Neurochemistry international. 2014;76:23–31. [PubMed: 24995391]

[91]. Kaur C, Ling EA. Effects of melatonin on macrophages/microglia in postnatal rat brain. J Pineal Res 1999;26:158–68. [PubMed: 10231729]

[92]. Galano A, Tan DX, Reiter RJ. Melatonin as a natural ally against oxidative stress: a physicochemical examination. Journal of Pineal Research. 2011;51:1–16. [PubMed: 21752095]

[93]. Espino J, Pariente JA, Rodriguez AB. Oxidative stress and immunosenescence: therapeutic effects of melatonin. Oxid Med Cell Longev 2012;2012:670294. [PubMed: 23346283]

[94]. Zhou J, Zhang S, Zhao X, Wei T. Melatonin impairs NADPH oxidase assembly and decreases superoxide anion production in microglia exposed to amyloid-beta1–42. J Pineal Res 2008;45:157–65. [PubMed: 18298462]

[95]. Das A, McDowell M, Pava MJ, Smith JA, Reiter RJ, Woodward JJ, et al. The inhibition of apoptosis by melatonin in VSC4.1 motoneurons exposed to oxidative stress, glutamate excitotoxicity, or TNF-alpha toxicity involves membrane melatonin receptors. J Pineal Res 2010;48:157–69. [PubMed: 20082663]

[96]. Douglas M, Stuart C, Sheryl K, Victor P. Correlations between histology and neuronal activity recorded by microelectrodes implanted chronically in the cerebral cortex. Journal of Neural Engineering. 2016;13:036012. [PubMed: 27108712]

[97]. Buzsaki G Large-scale recording of neuronal ensembles. Nature Neuroscience. 2004;7:446–51. [PubMed: 15114356]

[98]. Reiter RJ, Mayo JC, Tan DX, Sainz RM, Alatorre-Jimenez M, Qin L. Melatonin as an antioxidant: under promises but over delivers. J Pineal Res 2016;61:253–78. [PubMed: 27500468]

[99]. Agabiti-Rosei C, Favero G, De Ciuceis C, Rossini C, Porteri E, Rodella LF, et al. Effect of long-term treatment with melatonin on vascular markers of oxidative stress/inflammation and on the anticontractile activity of perivascular fat in aging mice. Hypertens Res 2017;40:41–50. [PubMed: 27534739]

[100]. Schmitt G, Schultze JW, Faßbender F, Buß G, Lüth H, Schöning MJ. Passivation and corrosion of microelectrode arrays. Electrochimica Acta 1999;44:3865–83.

[101]. Woeppel K, Yang Q, Cui XT. Recent advances in neural electrode-tissue interfaces. Current Opinion in Biomedical Engineering. 2017;4:21–31. [PubMed: 29423457]

[102]. Uttara B, Singh AV, Zamboni P, Mahajan RT. Oxidative stress and neurodegenerative diseases: a review of upstream and downstream antioxidant therapeutic options. Current neuropharmacology. 2009;7:65–74. [PubMed: 19721819]

[103]. Siomek A NF-kappaB signaling pathway and free radical impact. Acta Biochim Pol 2012;59:323–31. [PubMed: 22855720]

[104]. Kozai TDY, Marzullo TC, Hooi F, Langhals NB, Majewska AK, Brown EB, et al. Reduction of neurovascular damage resulting from microelectrode insertion into the cerebral cortex using in vivo two-photon mapping. J Neural Eng 2010;7:046011. [PubMed: 20644246]

[105]. Winslow BD, Christensen MB, Yang WK, Solzbacher F, Tresco PA. A comparison of the tissue response to chronically implanted Parylene-C-coated and uncoated planar silicon microelectrode arrays in rat cortex. Biomaterials. 2010;31:9163–72. [PubMed: 20561678]

[106]. Saxena T, Karumbaiah L, Gaupp EA, Patkar R, Patil K, Betancur M, et al. The impact of chronic blood-brain barrier breach on intracortical electrode function. Biomaterials. 2013;34:4703–13. [PubMed: 23562053]

[107]. Hu Y, Wang Z, Pan S, Zhang H, Fang M, Jiang H, et al. Melatonin protects against blood-brain barrier damage by inhibiting the TLR4/ NF-kB signaling pathway after LPS treatment in neonatal rats. Oncotarget. 2017;8:31638–54. [PubMed: 28404943]

[108]. Mazzetti S, Frigerio S, Gelati M, Salmaggi A, Vitellaro-Zuccarello L. Lycopersicon esculentum lectin: an effective and versatile endothelial marker of normal and tumoral blood vessels in the central nervous system. Eur J Histochem 2004;48:423–8. [PubMed: 15718209]

[109]. Robertson RT, Levine ST, Haynes SM, Gutierrez P, Baratta JL, Tan Z, et al. Use of labeled tomato lectin for imaging vasculature structures. Histochemistry and Cell Biology. 2015;143:225–34. [PubMed: 25534591]

[110]. Streit WJ, Kreutzberg GW. Lectin binding by resting and reactive microglia. J Neurocytol 1987;16:249–60. [PubMed: 3625239]

[111]. Donat CK, Scott G, Gentleman SM, Sastre M. Microglial Activation in Traumatic Brain Injury. Frontiers in Aging Neuroscience. 2017;9:208. [PubMed: 28701948]

[112]. Sullivan PG, Sebastian AH, Hall ED. Therapeutic window analysis of the neuroprotective effects of cyclosporine A after traumatic brain injury. Journal of neurotrauma. 2011;28:311–8. [PubMed: 21142667]

[113]. Horn KP, Busch SA, Hawthorne AL, van Rooijen N, Silver J. Another barrier to regeneration in the CNS: activated macrophages induce extensive retraction of dystrophic axons through direct physical interactions. The Journal of neuroscience : the official journal of the Society for Neuroscience. 2008;28:9330–41. [PubMed: 18799667]

[114]. Miron VE, Boyd A, Zhao J-W, Yuen TJ, Ruckh JM, Shadrach JL, et al. M2 microglia/ macrophages drive oligodendrocyte differentiation during CNS remyelination. Nature neuroscience. 2013;16:1211–8. [PubMed: 23872599]

[115]. Yu G-M, Kubota H, Okita M, Maeda T. The anti-inflammatory and antioxidant effects of melatonin on LPS-stimulated bovine mammary epithelial cells. PLOS ONE. 2017;12:e0178525. [PubMed: 28542575]

[116]. Baydas G, Reiter RJ, Yasar A, Tuzcu M, Akdemir I, Nedzvetskii VS. Melatonin reduces glial reactivity in the hippocampus, cortex, and cerebellum of streptozotocin-induced diabetic rats. Free Radical Bio Med 2003;35:797–804. [PubMed: 14583344]

[117]. Park S-W, Lee H-S, Sung M-S, Kim S-J. The Effect of Melatonin on Retinal Ganglion Cell Survival in Ischemic Retina. Chonnam Medical Journal. 2012;48:116–22. [PubMed: 22977753]

[118]. Ananth C, Gopalakrishnakone P, Kaur C. Protective role of melatonin in domoic acid-induced neuronal damage in the hippocampus of adult rats. Hippocampus. 2003;13:375–87. [PubMed: 12722978]

[119]. Jan JE, Hamilton D, Seward N, Fast DK, Freeman RD, Laudon M. Clinical trials of controlled-release melatonin in children with sleep-wake cycle disorders. J Pineal Res 2000;29:34–9. [PubMed: 10949538]

[120]. Potter KA, Buck AC, Self WK, Callanan ME, Sunil S, Capadona JR. The effect of resveratrol on neurodegeneration and blood brain barrier stability surrounding intracortical microelectrodes. Biomaterials. 2013;34:7001–15. [PubMed: 23791503]

[121]. Zhong Y, Bellamkonda RV. Dexamethasone-coated neural probes elicit attenuated inflammatory response and neuronal loss compared to uncoated neural probes. Brain research. 2007;1148:15–27. [PubMed: 17376408]

[122]. Walle T, Hsieh F, DeLegge MH, Oatis JE, Walle UK. HIGH ABSORPTION BUT VERY LOW BIOAVAILABILITY OF ORAL RESVERATROL IN HUMANS. Drug Metabolism and Disposition. 2004;32:1377–82. [PubMed: 15333514]

[123]. Shen Y, Cao B, Snyder NR, Woeppel KM, Eles JR, Cui XT. ROS responsive resveratrol delivery from LDLR peptide conjugated PLA-coated mesoporous silica nanoparticles across the blood-brain barrier. Journal of Nanobiotechnology. 2018;16:13. [PubMed: 29433522]

[124]. Bonnefont-Rousselot D, Collin F. Melatonin: Action as antioxidant and potential applications in human disease and aging. Toxicology. 2010;278:55–67. [PubMed: 20417677]

[125]. Buscemi N, Vandermeer B, Hooton N, Pandya R, Tjosvold L, Hartling L, et al. Efficacy and safety of exogenous melatonin for secondary sleep disorders and sleep disorders accompanying sleep restriction: meta-analysis. Bmj 2006;332:385. [PubMed: 16473858]

[126]. Nina B, Ben V, Nicola H, Rena P, Lisa T, Lisa H, et al. The Efficacy and Safety of Exogenous Melatonin for Primary Sleep Disorders. Journal of general internal medicine. 2005;20:1151–8. [PubMed: 16423108]

[127]. Posadzki PP, Bajpai R, Kyaw BM, Roberts NJ, Brzezinski A, Christopoulos GI, et al. Melatonin and health: an umbrella review of health outcomes and biological mechanisms of action. BMC Medicine. 2018;16:18. [PubMed: 29397794]

[128]. Jung-Hynes B, Reiter RJ, Ahmad N. Sirtuins, melatonin and circadian rhythms: building a bridge between aging and cancer. J Pineal Res 2010;48:9–19. [PubMed: 20025641]

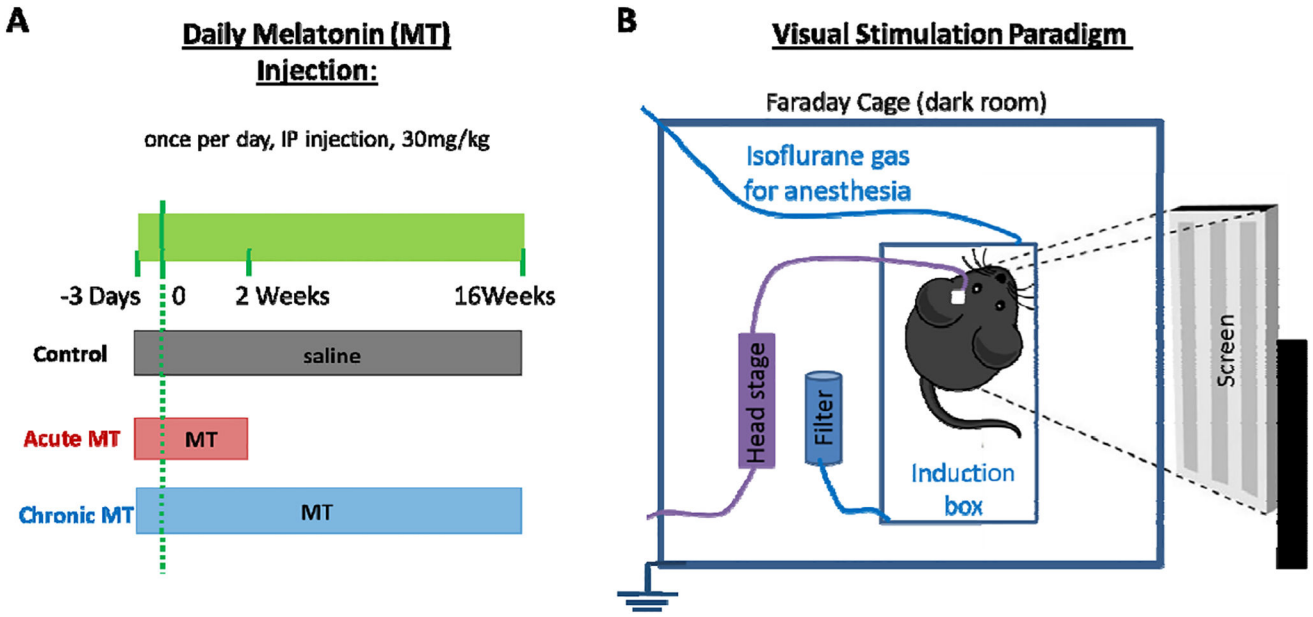

Figure 1. Experimental setup.

(**A**) Timetable of MT/saline injection in three groups (control, acute MT, and chronic MT) is illustrated. All injections went through i.p. injection, once a day. (**B**) Recording design. Animal is in a transparent isoflurane induction box inside of a Faraday cage. A 24" LCD screen is positioned outside of the cage.

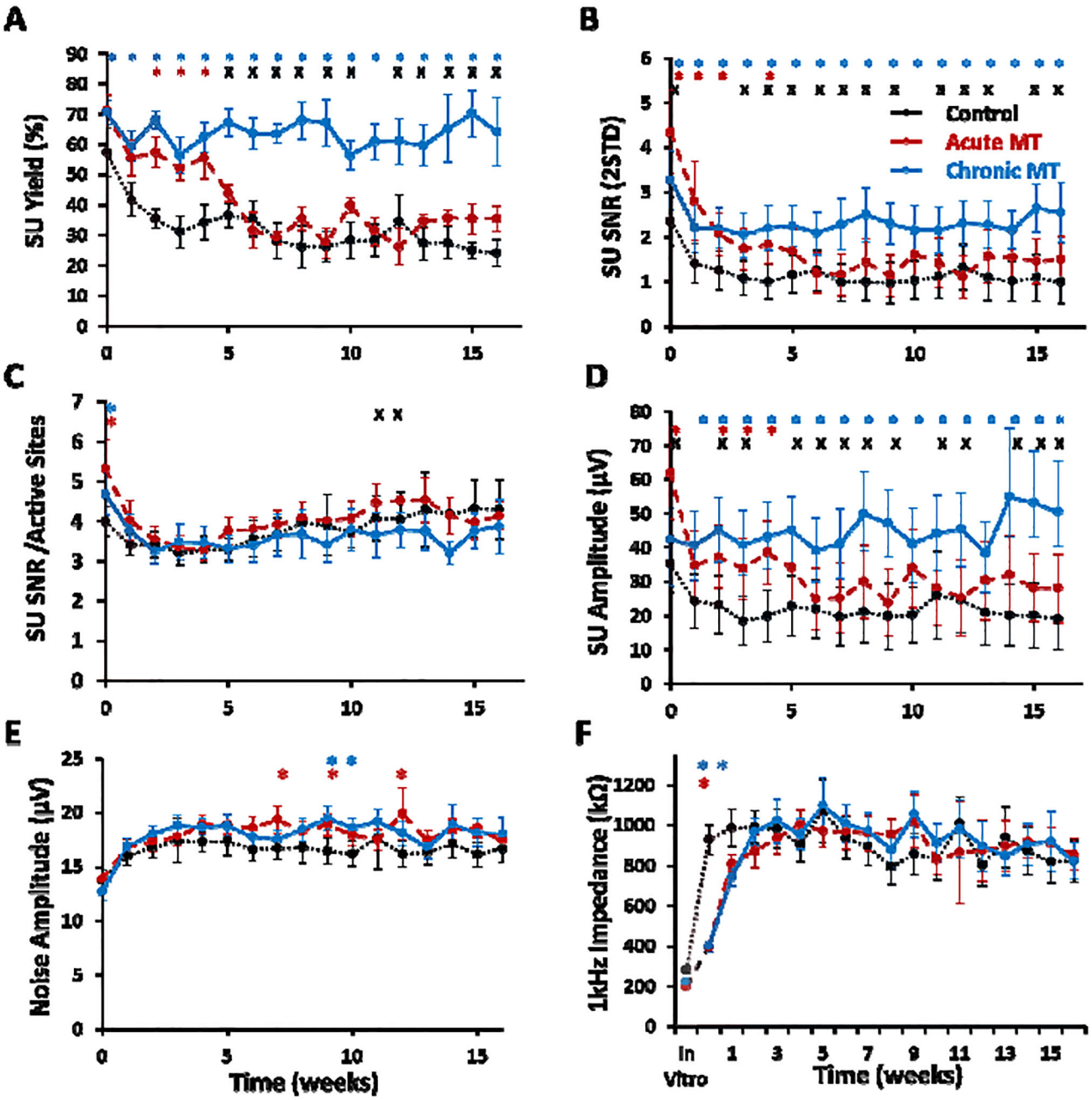

Figure 2. MT treatment improves chronic recording performance.

In vivo chronic neural electrode performance comparison between the control (black dotted), acute MT (red dashed), and chronic MT (blue solid) groups. Red shaded area shows the acute MT injection and blue shaded area presents the chronic MT injection. (**A**) Single-unit yield over 16 weeks post implantation. (**B**) Average SNR values (**C**) Average SNR of electrodes able to detect a single-unit. (**D**) Time evolution of average spike voltage amplitudes of single-units. (**E**) Average noise floor amplitude. (**F**) Average 1 kHz *in vitro* and *in vivo* impedance recorded every week post-implantation. All data presented as mean ± standard error of mean (SEM). Blue and red stars (*) and **x** represents $p<0.05$ for all. Blue *****

shows difference between the chronic MT vs control group. Red * presents difference between the acute MT and control animals, and **x** compares the acute MT vs chronic MT mice.

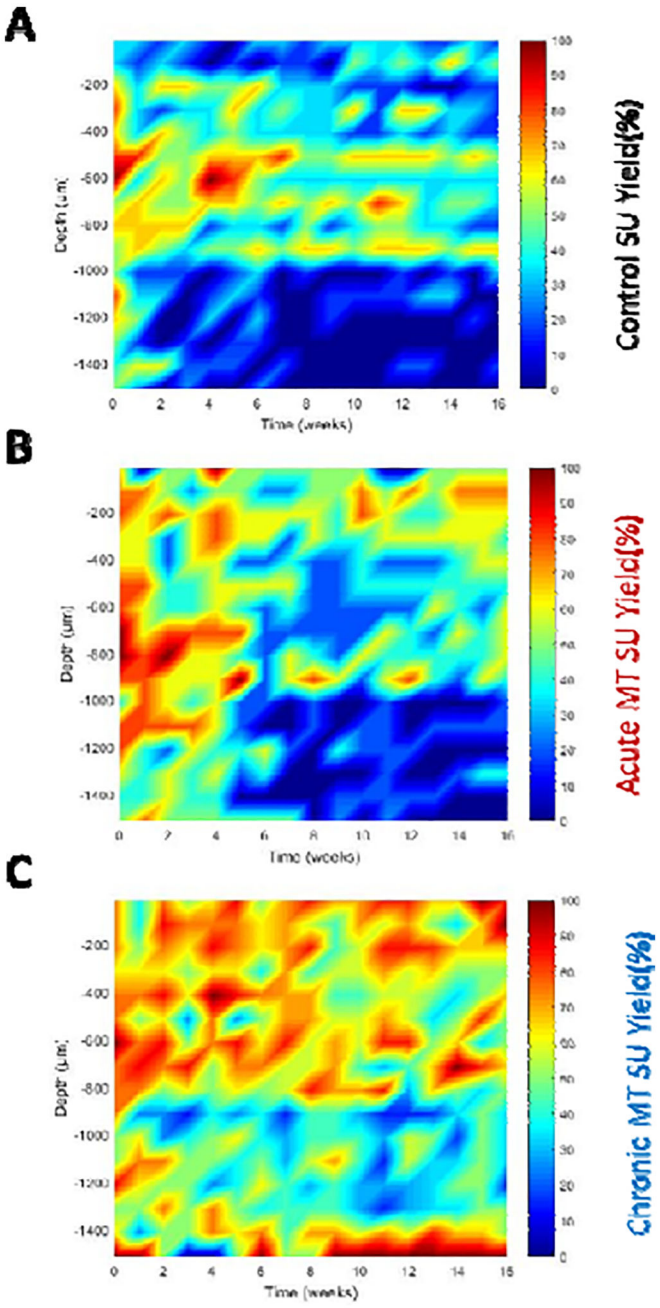

Figure 3. Single-unit yield recording performance as a function of depth and time.

Evoked SU yield electrode performance over time and implantation depth comparison between the control (**A**), acute MT (**B**), and chronic MT group (**C**). Note: higher yield is detected around 500 μm (layer IV) for all groups. Chronic MT group showed higher SU yield in many depths over time including the superficial (layer II/III), layer IV-VI and deeper regions (CA1).

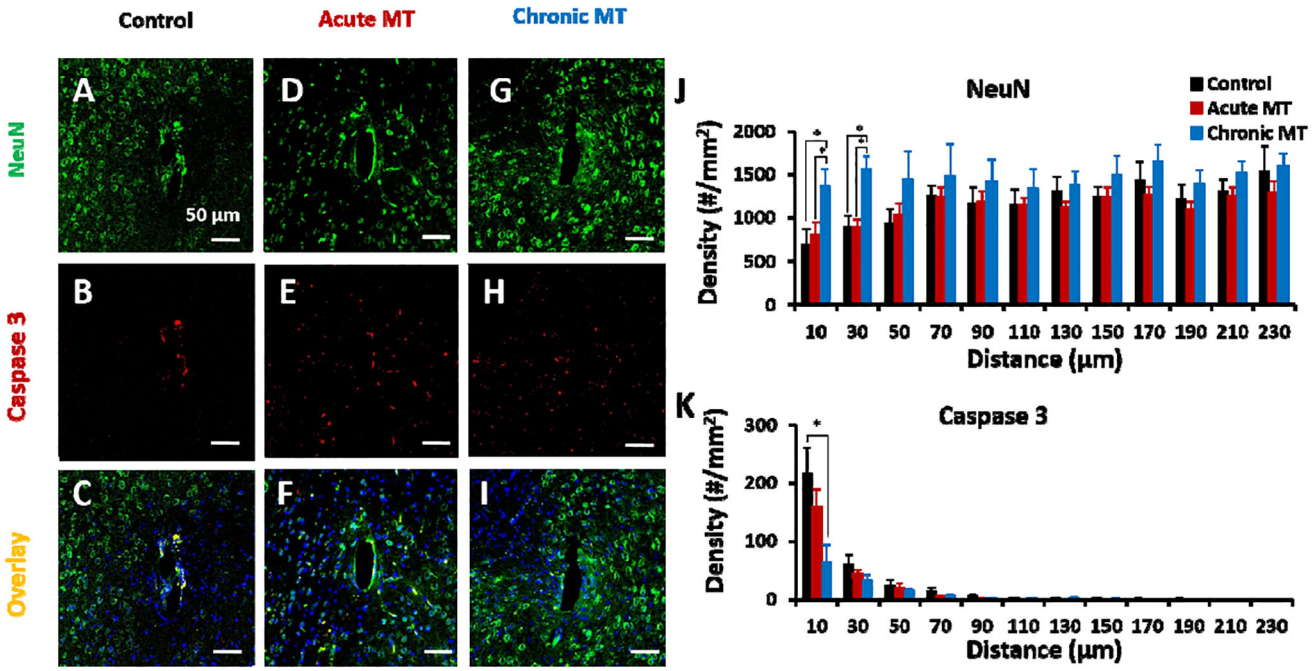

Figure 4. MT improves neuronal survival and reduces neurodegeneration.

Neuronal viability around implanted electrode in the control (**A-C**), acute MT (**D-F**) and chronic MT (**G-I**) mice showed limited co-localization of caspase-3 (**B,E,H**) and NeuN (**A,D,G**) in the chronic MT group at week 16. (**C,F,I**) are overlay of NeuN, caspase-3 and Hoechst in the control, acute MT and chronic MT groups, respectively. Scale bar in A-I, 50 µm. Cell density counts per mm^2 of neuronal cells (**J**) and caspase3-positive neuronal cells (**K**) at 16 weeks post-implantation is shown. (**J**) Neuronal cell counts were measured by automated analysis of NeuN staining. (**K**) Caspase 3-positive neuronal cells were measured by analysis of co-labeled cells with NeuN (control N=5 animal, N=8 sample; acute MT N=6 animal, N=8 samples, chronic MT N=6 animal, N=11 samples) and Caspase 3 (control N=4 animal, N=5 sample; acute MT N=4 animal, N=6 samples, chronic MT N=5 animal, N=7 samples) staining. Results were binned 10 µm from the electrode-tissue interface until 240 µm away, with 20 µm bin size. Data presented as mean ±SEM.

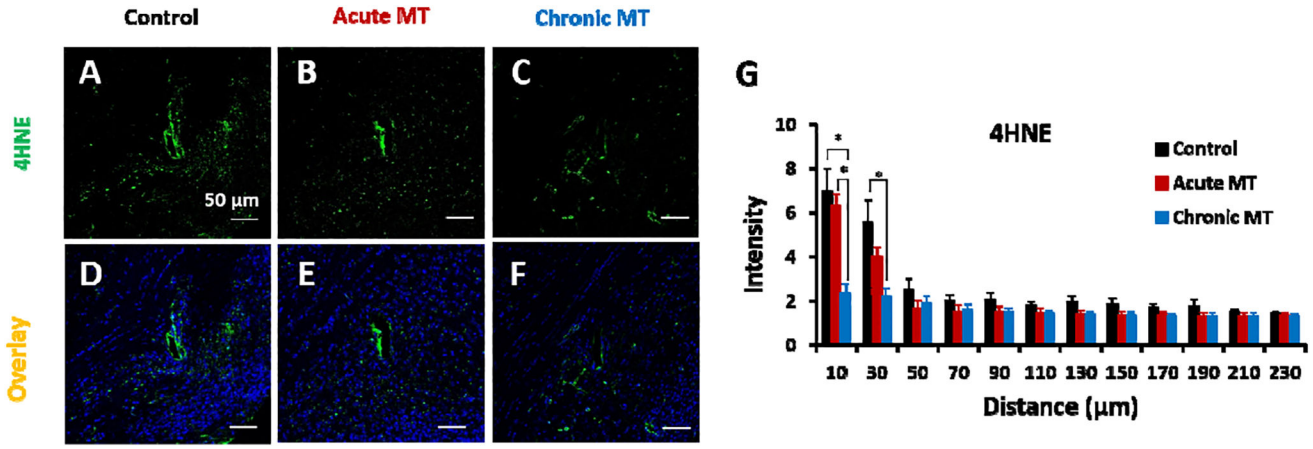

Figure 5. MT reduces oxidative stress.

(**A-C**) Representative immunohistochemical 4HNE staining (marker for lipid peroxidation, green) around implanted single shank electrode in the control, acute MT and chronic MT groups at week 16. (**D-F**) is the overlay images of 4HNE, with Hoechst. Scale bar in A-F, 50 µm. (**G**) is the normalized intensity values for 4HNE expression (histological samples for control N=5 animal, N=6 sample; acute MT N=6 animal, N=6 sample; chronic MT N=5 animal, N=6 sample). Intensities are calculated 10 µm from the implant site until 50 µm away, with 20 µm bin size. Data presented as mean ±SEM; * indicates $p<0.05$.

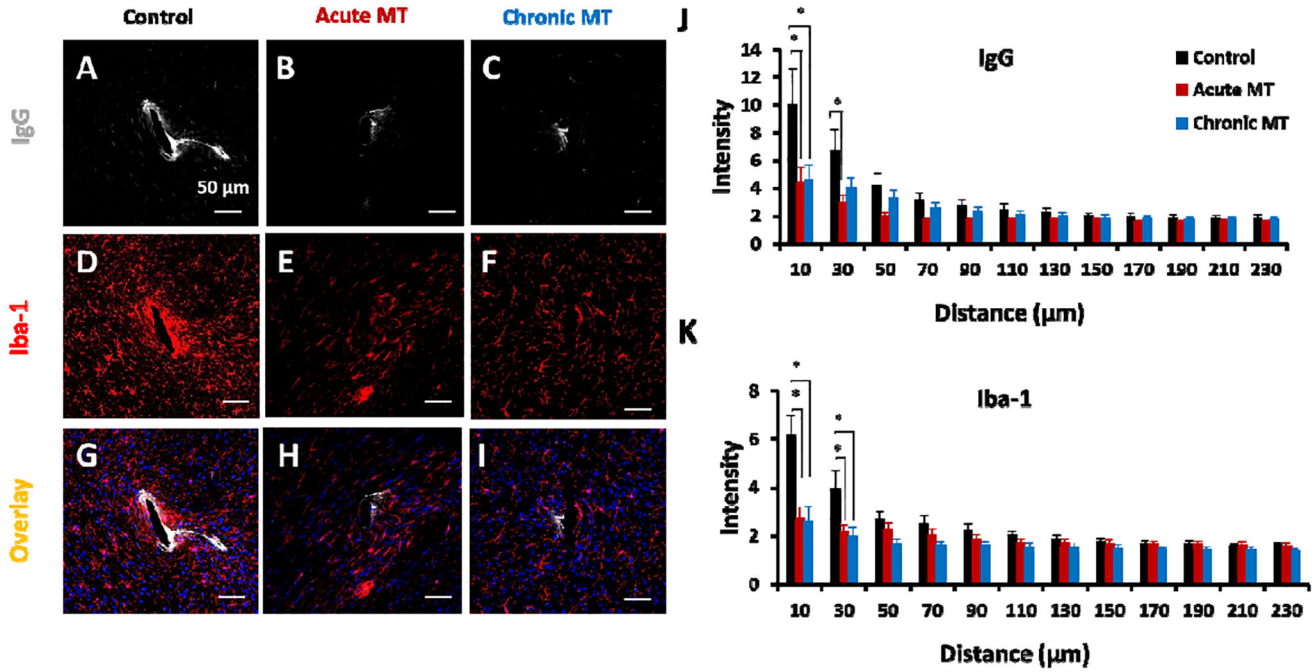

Figure 6. MT reduces chronic microglial activation and BBB leakage.

Representative Immunofluorescence examination of IgG (BBB leakage; **A-C**), and Iba-1 (microglia; **D-F**) around implanted electrode in the control, acute MT and chronic MT mice at week 16. (**G-I**) are the overlay images with Hoechst. Scale bar in A-I, 50 µm. (**J**,**K**) are the normalized intensity values for IgG and Iba-1 expression, respectively. Histological samples for IgG and Iba-1 staining (control N=5 animal, N=7 sample; acute MT N=5 animal, N=6 sample; chronic MT N=6 animal, N=7 sample). Intensities are calculated 10 µm from the implant site until 230 µm away, with 20 µm bin size. Data presented as mean ±SEM; * indicates $p<0.05$.

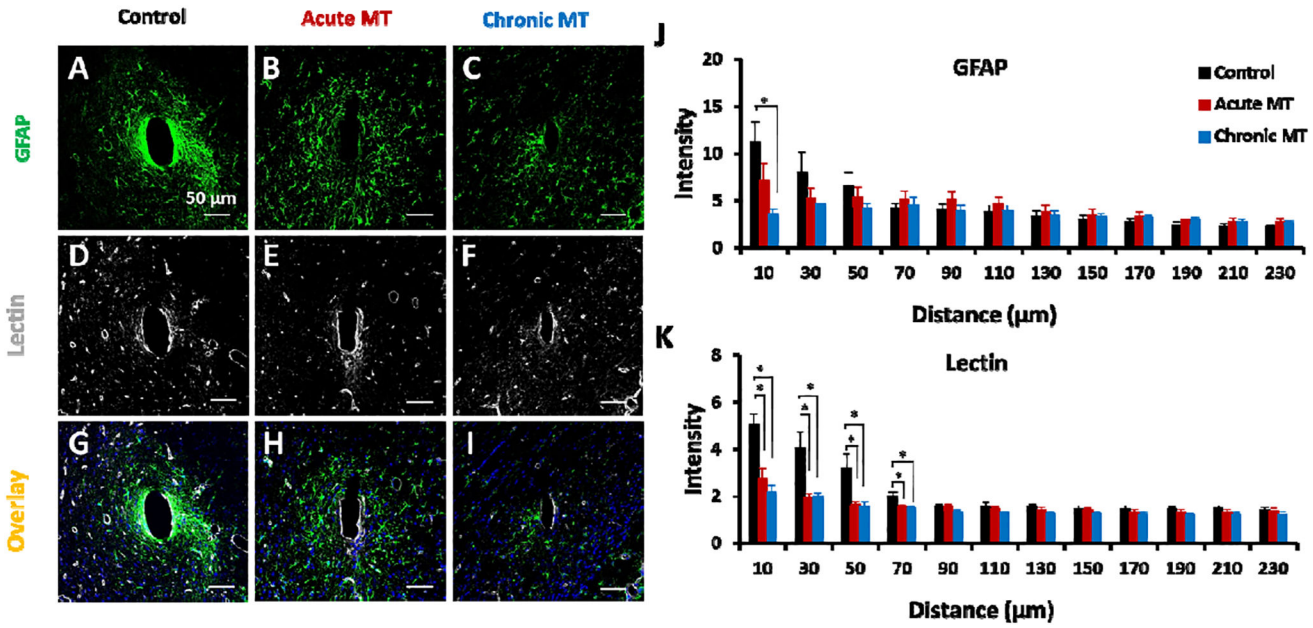

Figure 7. MT reduces Astrocyte activation.

GFAP (**A-C**) and tomato lectin (**D-F**) expression around implanted probe in the control, acute MT, and chronic MT mice at weeks 16. GFAP and lectin stain for astroglia and vascular endothelium, respectively. (**G-I**) are the co-labeled overlay images including Hoechst staining of control, acute MT and chronic MT Mice. Scale bar in A-I = 50 µm. (**J**,**K**) are the normalized intensity values for GFAP and lectin at week-16, respectively. Number of histological samples quantified for GFAP (control N=5 animal, N=10 sample; acute MT N=5 animal and N=6 sample; chronic MT N=6 animal and N=8 sample) and lectin (control N=5 animal, N=6 sample; acute MT N=6 animal and N=7 sample; chronic MT N=6 animal and N=4 sample). Intensities are calculated 10 µm from the probe-tissue interface until 240 µm away, with bin size of 20 µm. Data presented as mean ±SEM; * indicates $p<0.05$.

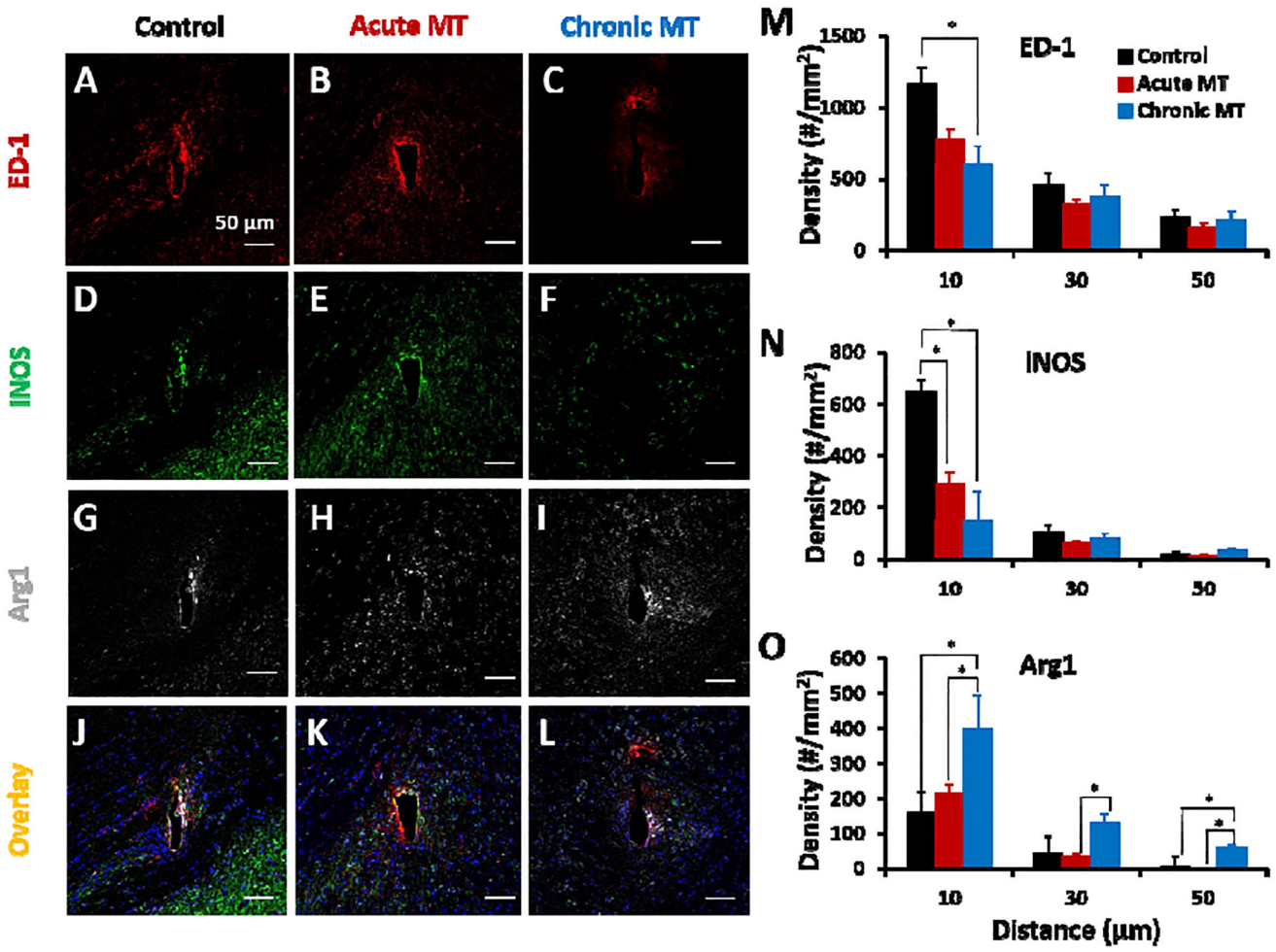

Figure 8. MT increases M2 macrophages and attenuates M1 macrophages.

Chronic immunohistochemical staining of ED-1 (activated macrophage/microglia; **A-C**), iNOS (M1 macrophages; **D-F**), Arg1 (M2 macrophages; **G-I**) response to the implantation of a silicon probe in the control, acute MT and chronic MT mice at week 16. (**J-L**) are the overlay images of ED1, iNOS, Arg1 with Hoechst. Scale bar in A-O, 50 µm. (**M**) is the density of activated macrophages (histological samples for control N=4 animal, N=6 sample; acute MT N=5 animal, N=12 sample; chronic MT N=6 animal, N=9 sample). (**N**) is the density of co-labeled iNOS-ED1 macrophages and (**O**) is the density of co-labeled Arg1-ED1 macrophages. Densities are calculated 10 µm from the implant site until 50 µm away, with 20 µm bin size. Data presented as mean ±SEM; * indicates $p<0.05$.

Table 1.

Antibodies used for immunohistochemistry characterization

Antibody	Specificity
NeuN	Neurons
Caspase-3	Apoptotic cell death
GFAP	Astrocytes
Iba-1	Microglia
IgG	BBB leakage
Lectin	Blood vessels
iNOS	M1 macrophage
Arg1	M2 macrophage
ED-1	Macrophage/microglia
4HNE	Lipid peroxidation